REGENERATIVE PERIPHERAL NERVE INTERFACING OF SENSORY MODALITIES

by

NILANJANA T DUTTA

Presented to the Faculty of the Graduate School of

The University of Texas at Arlington in Partial Fulfillment

of the Requirements

for the Degree of

MASTER OF SCIENCE IN BIOMEDICAL ENGINEERING

THE UNIVERSITY OF TEXAS AT ARLINGTON

December 2012

Acknowledgements

I am immensely pleased to place on record my profound gratitude and heartfelt thanks to my supervisor, Dr. Mario Ignacio Romero-Ortega , for his guidance during my research, who suggested the problem, extended all facilities and provided inspiring guidance for the successful completion of my research work. I deem it as my privilege to be given an opportunity to work in the field of Neuroscience, under his able guidance.

I want to convey my sincere gratitude to Dr. Khosrow Behbehani and Dr. Samarendra Mohanty for agreeing to be a part of my committee. I also want to thank them for their support and suggestions at different points of time during my Master's degree.

I do thank all teaching and non-teaching staff, with special gratitude to Dr. Liping Tang and Dr. Jennifer L. Seifert, from Department of Biomedical Engineering at the University of Texas Arlington, for all the help they rendered me during my studies and research here as a Master's student.

I would like to express my eternal appreciation towards my parents and my husband who have always been there for me no matter where I am, for the constant motivation and all unconditional support and patience, with particular mention to my father's 'open 24X7 helpline'. I also want to extend a special thank you to my brother-in-law for his valuable inputs and suggestions during the entire process. Thank you for being ever so understanding and supportive.

I would like to thank my dear friends and colleagues, especially fellow lab mates. It has been wonderful knowing you all during my time here at UTA.

November 19, 2012.

Abstract

REGENERATIVE PERIPHERAL NERVE

INTERFACING OF SENSORY

MODALITIES

Nilanjana T Dutta, MS

The University of Texas at Arlington, 2012

Supervising Professor: Mario Ignacio Romero-Ortega

Peripheral neural interfaces (PNI) has proved potential to record motor commands for the control of these prosthetic limbs, together with stimulation of specific sensory axons, so as to transmit specific sensory sub-modalities. Although PNI is hypothesized to provide adequate sensory feedback, realizing this degree of specificity is not fully established. Recently, a regenerative multi-electrode interface (REMI) was reported to be capable of recording peripheral nerve activity from a transected nerve.

This study is aimed at interfacing neural activity specific to sensory sub-modalities, such as thermal pain, mechanoception and limb stretching using the REMI, in a freely moving animal. In the experiment, a floating multi-electrode array comprising 18 Platinum/Iridium electrodes encased within a collagen-filled hollow polyurethane tube was implanted in female adult Lewis rats. Surgery involved transection of the mixed sciatic nerve followed by suturing of nerve stumps to the conduit. Neural activity was recorded every week using Omniplex data acquisition system (Plexon Inc. USA) equipped with live Cineplex video tracking, during various sensory tests like Plantar Von Frey stimulation (mechanoception), Plantar thermal (nociception) and wake/resting (Control). Extracellular spikes (single/multi-unit) were recorded weekly, from

regenerating axons beginning from 7 days to 42 days post implantation, with high signal to noise ratio (up to 7.98:1). The neural activity was evaluated in terms of different parameters, such as: firing rate, amplitude and wave-shape, known to encode the stimulus properties in the sensory system. Results demonstrate that single unit spikes recorded at early time points of 7-21 days were possibly from unmyelinated fibers with incomplete re-innervation accounting for spontaneous discharge, on the other hand neural activity at 28 days through 42 days were more correlated to the evoked sensory response during stimulation and the motor response due to paw withdrawal. However, average recorded channels per animal decreased in number from 35% at 14days to 12.5% at 42 days (i.e. approx. 5% reduction every week) due to mechanical device failures, causing statistically insignificant number of samples by 42 days. Neural activity was first categorized by the discharge pattern observed during sensory behavioral tests into spontaneous, random and burst pattern. Further evaluation was done by the wave shape into monophasic, biphasic and triphasic units. However, recording at these early time points from a mixed regenerating nerve lead to inconclusive results as the stimulation causes successive activation of numerous nerve fibers. Similar assessment, based on the wave shape parameters and firing pattern was used to evaluate the immediate effect of cyclic stretching of the interfaced limb resulted in insignificant change (<20%) with reference to the recorded neural activity prior to stretching.

Table of Contents

List of Illustrations

List of Tables

Chapter 1

Introduction

1.1 Limb Loss and Amputation

The World Health Organization have approximated that Latin America, Africa, and Asia together have almost 30 million people in need of prosthetic limbs, braces, or other devices (Aleccia 2010). In the United States alone there are more than 2 million people living with limb loss and the numbers are still growing. Nearly 507 amputations are done daily across the United States (Graham K et al. 2008). Limb Loss may be caused by natural life threatening diseases like diabetes and cancer or due catastrophic personal injury like war and accidents result severe, non-recoverable damage or immediate loss of the extremities when the incident occurs, as illustrated in Figure 0.1. As per the information from the National Institute of Diabetes and Digestive and Kidney Diseases (NIDDK) division of the National Institutes of Health, more than 50% of all lower-limb amputations in the United States occur in people who are Diabetic, accounting for 86,000 amputations each year. As of September 1, 2010, there were 1222 major limb amputations from Operation Enduring Freedom and Operation Iraqi Freedom treated in all U.S. military facilities with 21% accounting for major upper extremity loss. (U.S. Military Casualty Statistics: Operation New Dawn, Operation Iraqi Freedom, and Operation Enduring Freedom, Hannah Fischer, Congressional Research Service September 28, 2010). Despite recent development in robotic prosthesis to facilitate people with these special needs, functioning normally and effectively with a missing limb is still a challenge.

Among the millions of people suffering from limb amputation, approximately 30 percent account for upper limb loss alone. The limb amputation is classified by the level of injury, that include loss of one or more fingers (trans-metacarpal) and can be as severe

as the loss of an entire arm (shoulder disarticulation) (Figure 0.2: Levels of Limb Amputation). Approximately 70 percent of all upper limb loss is amputations distal to the elbow.

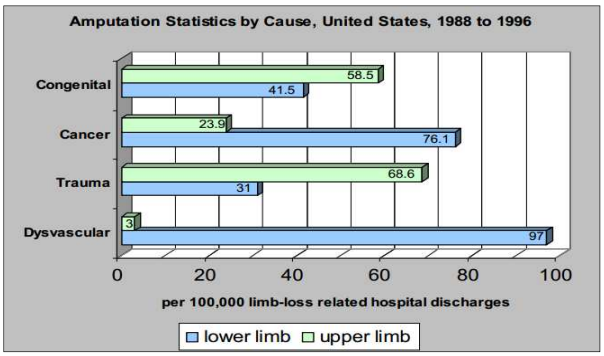

Figure 0.1: Statistics of Amputations in the United States of America by Cause of Occurrence (Dillingham et al. 2002)

However, any degree of upper limb amputation greater than Trans-carpal disarticulation, will contribute to the complete loss of sensation from the hand. Therefore there is a continuous and growing need to develop enhanced artificial limbs so that the affected people can lead as normal a life as possible.

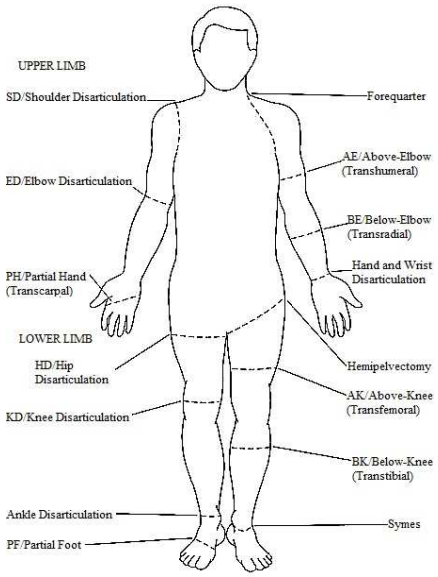

Figure 0.2: Levels of Limb Amputation (adapted from Aleccia 2010)

1.2 Underlying Anatomy and Physiology

The upper extremity operates as a complete system which coordinate movements to create overall mobility and dexterity, with the hand contributing about 90% of the function alone (Magee 1997). The Human hand is an organ with the capacity and versatility to perform numerous motor, sensory and tasks incorporating a combination of the two for haptic perception (Flanagan et al. 2002) with unequaled proprioceptive and sensory feedback capabilities. The six prehensile grip postures that are naturally adopted by the hand for undertaking various tasks are illustrated in Figure 0.3.

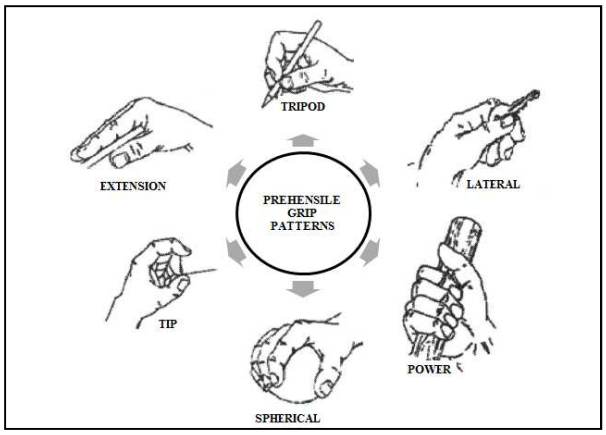

Figure 0.3: Prehensile Grip Patterns (adapted from Light et al. 2002)

Skin, muscles, joints and all other peripheral tissues are innervated by different classes of afferent nerve fibers each transducing and encoding specific stimulus characteristics they are sensitive to, and by the target organ and distributions of their central projections and peripheral terminations (Vernon 2005). Some of the fibers terminate as specialized sensory end organs and other thin fibers end freely. Collectively, they form an overlapping spatial and temporal architecture of receptors which provides selective transducing functions, like mechanical, chemical and/or thermal (Vernon 2005).

The sensory fibers innervating the hand of humans vary from the largest Aα-fibers (70-120 m/s) that innervate the muscle spindles of the hand, to the unmyelinated C-fiber, polymodal nociceptive fibers saturating all tissues of the hand but the bone (Kandel 2000).

The glabrous skin of the palm and palmar surfaces of the fingers is innervated by four kinds of thicker, myelinated Aβ fibres that conduct in the range of 25–75 m/s and end specifically in specialized non-neural cells of Meissner corpuscles, Pacinian corpuscles, Merkel cell–neurite complexes or Ruffini corpuscles. These fibers are all sensitive to skin stimulation ranging from low threshold to non-noxious mechanical and grade their firing frequency with respect to the intensity of stimulus. Those linked to Meissner or Pacinian

corpuscles are rapidly adapting and mainly discharge at the onset or offset of stimulus thus indicating stimulus transients like contact, movement, velocity and vibration. In humans, stimulation of recognized Meissner corpuscles evokes low frequency vibration and sensations of stimuli movement. On the contrary, stimulation of Pacinian afferents evokes sensations high frequency, vibration of contact and movement. The slow adapting fibers associated to Merkel cell–neurite complexes and Ruffini corpuscles, discharge at the onset of stimulation and continue firing throughout the application of stimulus indicating continuity such as pressure, displacement and skin stretch. Merkel cells are associated to sensations of contact, pressure, texture and two-dimensional form evoked in afferents whereas Ruffini afferents are associated to no obvious sensations in humans (Vernon 2005).

The other nerve fibers, for instance thinly myelinated Aδ fibers (5–40 m/s) and unmyelinated C fibers (0.5–2 m/s) form specific receptor classes for cooling, warming, noxious heat or cold, destructive mechanical or mixed noxious stimuli. These receptors are comparatively insensitive to innocuous low-threshold mechanical stimuli transduced by the Aβ fibers and discharge at mechanical thresholds only after Aβ fibers are firing at maximal rates. These isolated fibers are capable of evoking sensations in response to coolness, warmth, intense mechanical pain, cold pain, heat pain or slow burning pain, but with an emphasis on pricking pain at short latency for the Aδ fibers and on slow, burning but accurately localized pain for the C fibers (Vernon 2005).

Table 0.1: Receptor types active in somatic sensation (Kandel et al. 2000)

Receptor type	Fiber groups[1]	Fiber name[1]	Modality
Cutaneous and subcutaneous mechanoreceptors			Touch
Meissner's corpuscle	Aα,β	RA	Stroking, fluttering
Merkel disk receptor	Aα,β	SAI	Pressure, texture
Pacinian corpuscle[2]	Aα,β	PC	Vibration
Ruffini ending	Aα,β	SAII	Skin stretch
Hair-tylotrich, hair-guard	Aα,β	G1, G2	Stroking, fluttering
Hair-down	Aδ	D	Light stroking
Field	Aα,β	F	Skin stretch
Thermal receptors			Temperature
Cool receptors	Aδ	III	Skin cooling (25°C)
Warm receptors	C	IV	Skin warming (41°C)
Heat nociceptors	Aδ	III	Hot temperatures (>45°C)
Cold nociceptors	C	IV	Cold temperatures (<5°C)
Nociceptors			Pain
Mechanical	Aδ	III	Sharp, pricking pain
Thermal-mechanical	Aδ	III	Burning pain
Thermal-mechanical	C	IV	Freezing pain
Polymodal	C	IV	Slow, burning pain
Muscle and skeletal mechanoreceptors			Limb proprioception
Muscle spindle primary	Aα	Ia	Muscle length and speed
Muscle spindle secondary	Aβ	II	Muscle stretch
Golgi tendon organ	Aα	Ib	Muscle contraction
Joint capsule mechanoreceptors	Aβ	II	Joint angle
Stretch-sensitive free endings	Aδ	III	Excess stretch or force

The peripheral system serves the tactile skin sensation by a population of approximately 70 units/cm^2, of low threshold mechanoreceptive units that are sensitive to skin deformation (Johansson et al. 1979), with the density increasing in the distal direction of the hand and highest concentration in the fingertips (Flanagan et al. 2002). Table 0.1 illustrates different nerve fibre types and associated sensory receptors.

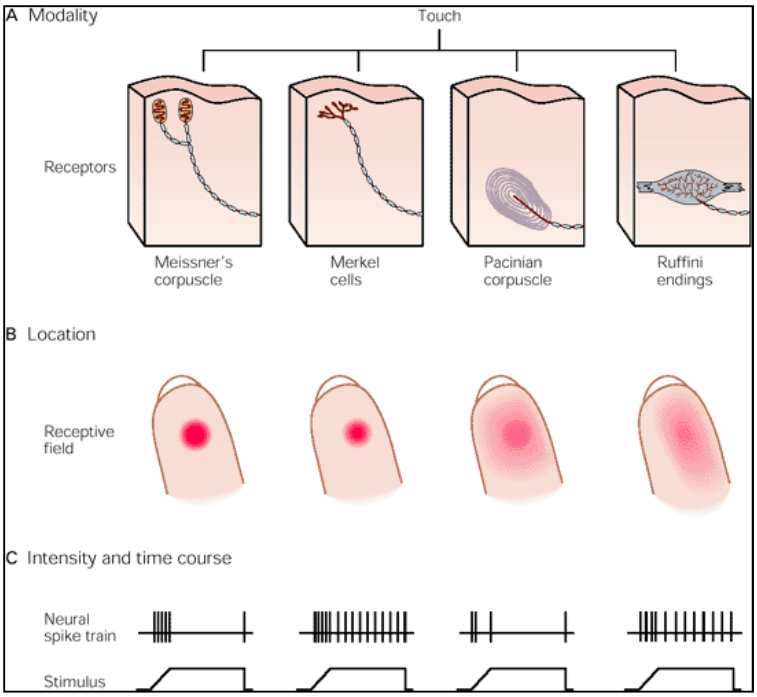

Figure 0.4: The sensory systems encode 4 elementary attributes of stimuli—modality, location, intensity and timing for the somatosensory modality of touch (Kandel et al. 2000)

Thus nerve fibers can be classified based on their fiber diameter and conduction velocity (CV), namely: Aα efferent motor (12-22 μm), Aβ proprioceptive (5-12 μm), Aδ motor fibers innervating muscle spindles (1-5 μm), and C fibers for noxious heat and pricking pain perception (0.1-1.3 μm) (Parent et al. 1996). In mammals, the classification defines that the motor nerves are composed of Aα, Aβ, Aδ and c fibers and pure sensory nerves are composed of the Aβ, Aδ and c components (Manzano et al. 2008).

1.2.1 Organization of Peripheral Nervous System

The PNS includes neuronal cell bodies located in the spinal cord or within the Spinal Ganglia (Dorsal Root and Ventral Root Ganglia), their central connections (nerve roots), and their axons extending as peripheral nerves (myelinated and unmyelinated) to innervate into the target organs (i.e. skin, muscle)(Figure 0.5A). A typical nerve constitutes of both afferent and efferent nerve fibers grouped in fascicles enclosed within

layers of connective tissue (Peters et al. 1991). The architecture of fascicles transforms throughout the length of the nerve with a growing number of fascicles of smaller size in distal with respect to proximal segments. The peripheral nerves are composed of three supportive sheaths: epineurium, perineurium, and endoneurium. The epineurium is a layer of loose connective tissue with blood vessels that supply the nerve. The perineurium, mainly made of layers of flat perineurial cells surrounded by an outer layer of longitudinal, circumferential, and oblique bundles of collagen fibers, is the diffusion barrier maintaining the endoneurial fluid pressure and contributes majorly to the tensile strength of the nerve. The middle layer, composed of fibroblasts, collagen and reticular fibers, and extracellular matrix, is called the endoneurium. The endoneurial collagen fibrils form the walls around nerve fibers within the fascicle. Axons of nerve fibers maybe surrounded by Schwann cells (myelination) inside the endoneurial tubules (Navarro et al. 2005) (Figure 0.5B).

Each Schwann cell and its associated myelin provide electrical insulation and encase a histologically distinct zone called internodes (Ducker et al. 1972 and Duncan et al. 1980). The gap between two internodes, Nodes of Ranvier are selectively permeable to extracellular ions, facilitating rapid nerve impulse conduction. The increased transmembrane potential due to myelination results in an impulse conduction occurring only at the nodes classified as saltatory conduction and not along the entire length of the nerve (Figure 0.6). Myelination assists in accomplishing conduction with fewer ions and furthermore allowing more rapid repolarization with minimal energy expenditure (Duncan et al. 1980 and Guyton et al. 1976).

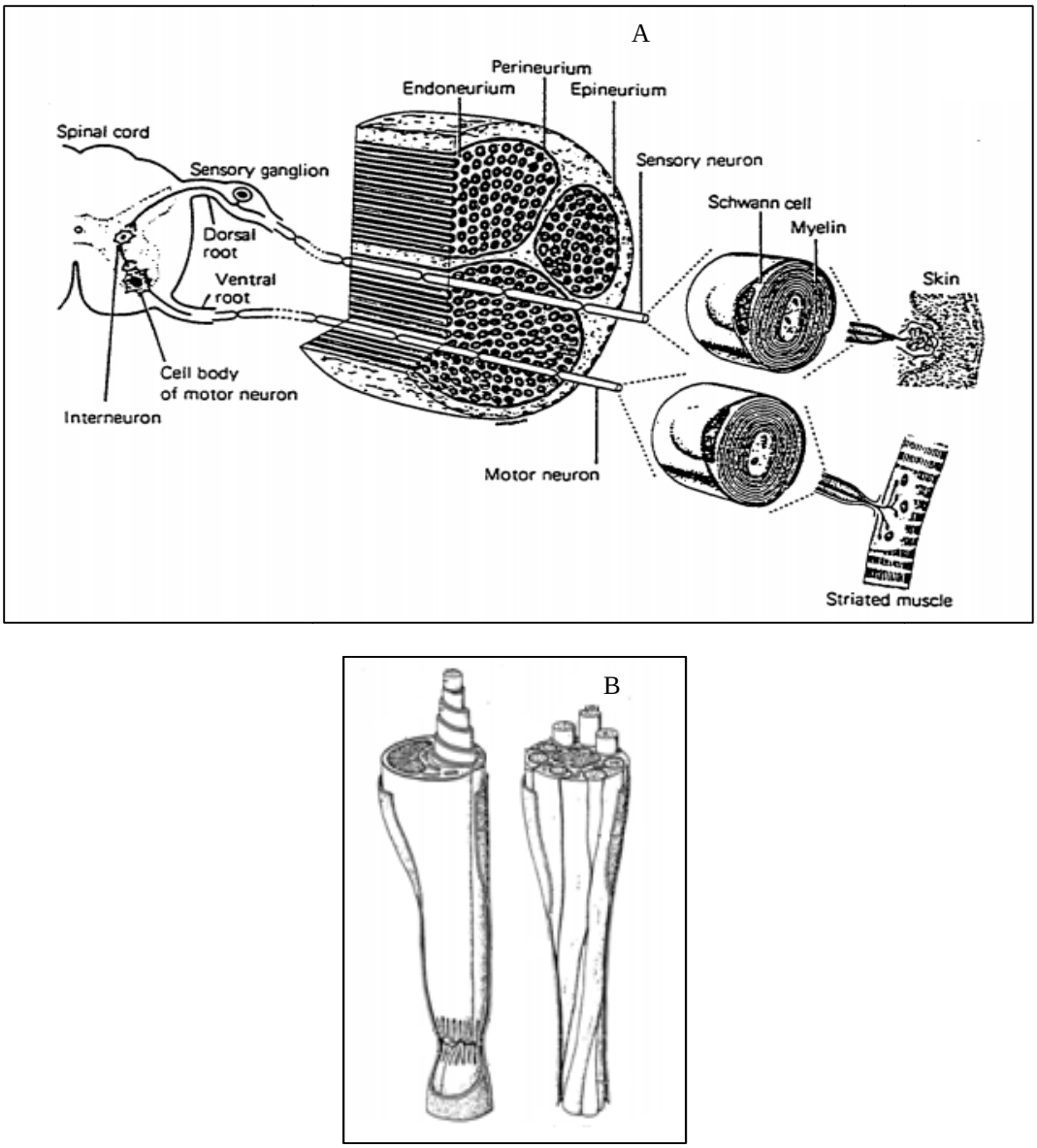

Figure 0.5: (A) Organization of Peripheral Nerve, (B) Myelinated (left) and Unmyelinated (right) Nerve Fibers (Benke 1989)

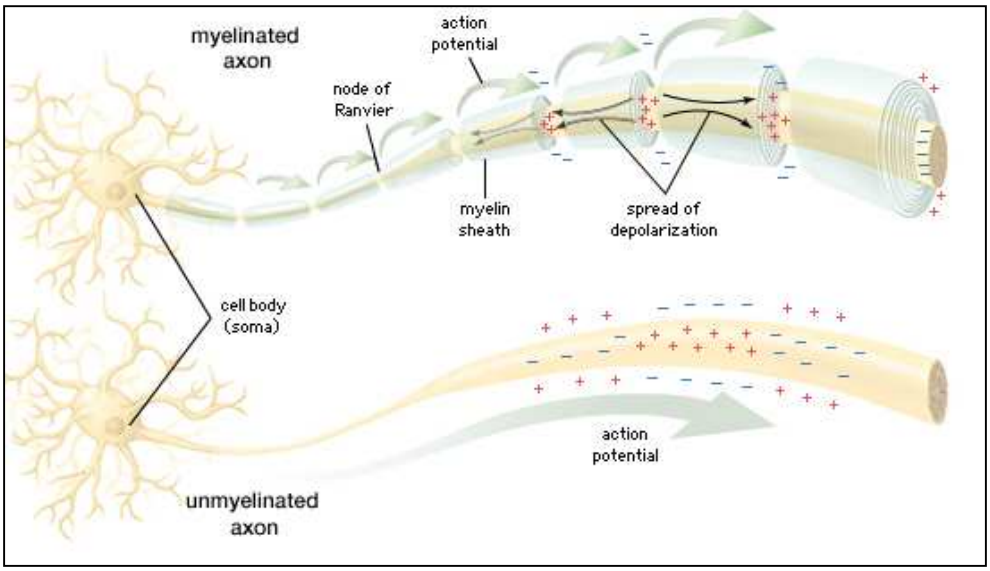

Figure 0.6: Schematic showing conduction of action potential: Myelinated axon showing saltatory conduction (above), Unmyelinated axon showing impulse propagation along the length of the nerve (below)

Alternatively, in unmyelinated axons, membrane along the entire length of nerve is involved in impulse propagation via flow of ion exchange, described as an eddy current across the cell membrane surface. Speed of depolarization is governed by axon cross-sectional diameter, i.e. Larger cross-sectional diameter allows larger current flow and faster local excitation thus resulting higher conduction velocity (Eyzaguirre et al. 1975 and Guyton et al. 1976).

1.3 Upper limb Prosthesis

Traditionally, prosthetic arms were nothing more than hook and cable devices providing limited movement as opposed to a normal hand with 27 degrees of freedom (ElKoura et al. 2003). These devices consisted of a simple hook as the hand (Figure 0.7), which is operated manually to open and close, and a harness wrapped around the shoulder of the undamaged arm. This prosthesis can move in three different directions only, leading to be not so effective and causing discomfort to the person wearing the

device. Therefore (hand and/or hook) offered very little in the way of true functional restoration to individuals with upper limb deficiencies (Billock et al. 1986).

Figure 0.7: Photograph of terminal devices: Hooks and Prehensors (Courtesy Maj. Underwood)

Recent development in the field of robotic prosthesis has revealed the DEKA arm (Figure 0.8A), designed by Dean Kamen, is intended to be a non-invasive solution for amputees which incorporates numerous circuits and microprocessors within the arm allowing for greater range of motion and reception of thoughts from the user's brain to simulate chest muscles. DEKA arm is operated based on the targeted re-innervation concept described in section 1.4.1.1. Hence the pectoral "muscles" will contract and relax based on the information they receive from the brain, to control the prosthetic arm movement. It has the capacity to provide 10 degrees of freedom and sensors on the fingertips of the hand enable detection of the grip strength on an object but not temperature or texture (Adee 2008). Another comparable device is the PROTO 2 arm (Figure 0.8B) designed by DARPA which imitates the mechanics of the human arm with its wide range of motion, and power capabilities. This arm employs two lightweight "bones" made of carbon fiber and aluminum alloys and has the capacity to perform 25 joint motions (Adee 2008), for example the shoulder and wrist are capable of roll, pitch and yaw, the elbow can flex, and the fingers and thumbs bend at each knuckle.

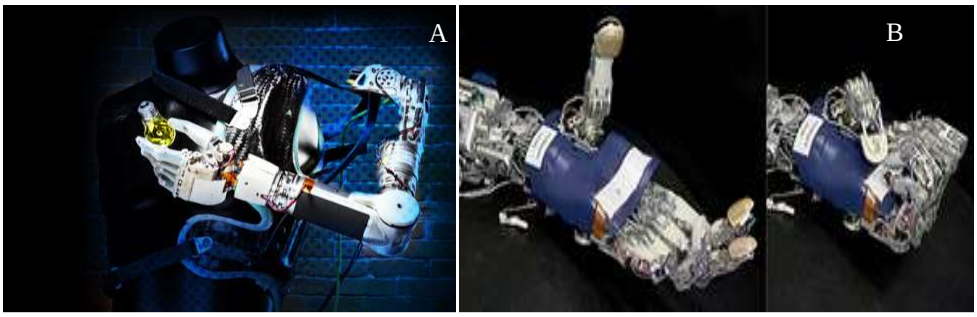

Figure 0.8: Photographs for (A) DEKA arm (courtesy DEKA), (B) Proto 2 Hand Movements (courtesy Johns Hopkins University)

1.4 Prostheses Control

1.4.1 Open Loop Control

Current muscle controlled functional prostheses for upper limb amputees can be categorized in three groups namely body-powered (no outside power source), myoelectric (electrically controlled) and Targeted Muscle Reinnervation. Body-powered prostheses mainly operate via a mechanical system of cables, harness and manual control using exaggerated residual body movements to pull on the cable and successively perform a prosthetic operation (Fletcher et al. 1970, Vitali et al. 1978). However, this system functions effectively with significant strength and control of shoulder, chest and the residual limb and provides limited range of motion (Billock et al. 1986). The second category is myoelectric prostheses. They are motorized and are controlled via surface electromyogram (EMG) signals from residual muscles sites. The controlling of this prosthesis is commonly achieved by detecting activity from two independent muscles or by differentiating weak and strong contractions of one muscle (Herberts et al 1980, Stein et al. 1983). This type offers a wider range of motion and higher grip strength. Conversely, recording suitable and isolated EMG signals and moreover making repeatable contractions is complex, thus causing a shortage of information for control of various functions (Micera et al. 2010). A combination of the

operative principle of the body-powered type and the control mechanism of the myoelectric type is incorporated in the hybrid prostheses. Nevertheless these systems include limited or no prehension feedback and control limited to one movement at a time, lack of sensory feedback leading to differences in control and body image integration between a natural limb and a prosthetic limb (Behrend et al. 2011).

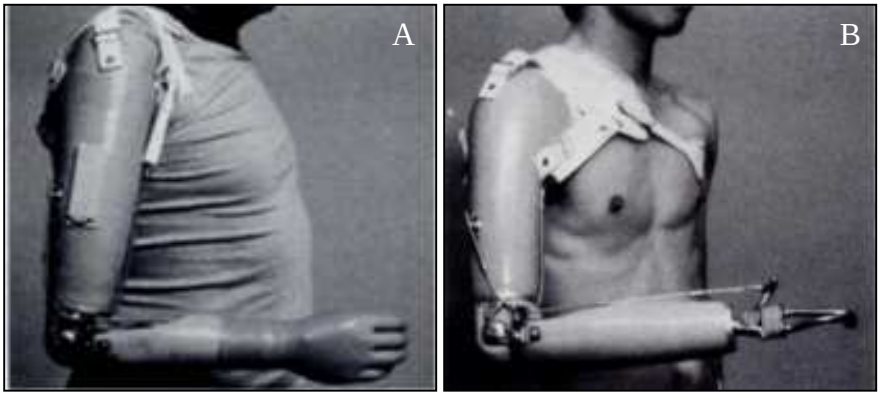

Figure 0.9: (A) An above-elbow amputee fitted with a hybrid prosthesis, a myoelectric hand and a cable-operated elbow unit in an internal locking mechanism, (B) Body powered prosthesis in above elbow amputee (Heger et al. 1985)

However, these can be overcome with Targeted reinnervation as it increases the amount of information available from muscles, permitting the control of multiple prosthetic functions.

1.4.1.1 Targeted Muscle Reinnervation

Targeted muscle hyper-reinnervated, a technique examined in rats, was developed by Dr. Todd Kuiken in 1995. This method involves remapping large nerves containing many motor neurons onto a small muscle area to hyper-reinnervate the muscle, which in turn allows the muscle to be controlled using signals from the transferred nerve. (Kuiken et al. 1995).

The first successful TMR procedure was performed on a human patient with trans-humeral and shoulder disarticulation amputation in 2006 (Jeffrey et al 2007). It is a

technique to improve the control of myoelectric prostheses. This new surgical process incorporated the denervation of the biomechanically non-functional residual chest muscle in an amputated patient (Kuiken et al. 2003, Kuiken et al. 2004, Hijjawi et al. 2006 and Kuiken et al. 2006)(Figure 0.10). The original nerves of the target muscle, which were cut and/or de-activated, are then reinnervated with residual stumps of nerves of the amputated limb. The resultant EMG signals of the targeted muscle provide physiologically appropriate EMG signals for motor commands to the missing limb, and thus drive a motorized prosthetic device.

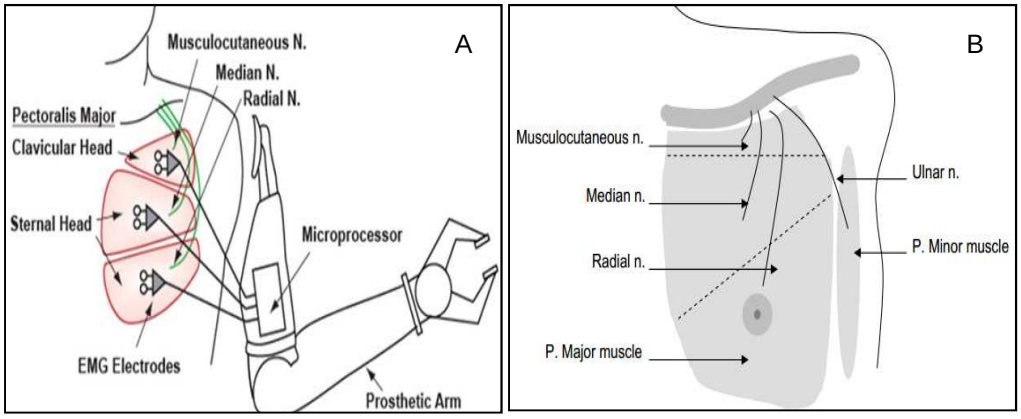

Figure 0.10:Schematic of targeted muscle reinnervation for improved myoelectric prosthesis control in bilateral shoulder disarticulation amputee. (A) Electromyograph electrode placement for operating a programmed prosthetic arm (B) Pectoralis major reinnervation by four major arm nerves. (Adapted from Kuiken et al. 2004)

1.4.2 Closed Loop Prosthetics

1.4.2.1 Targeted Sensory Reinnervation

Targeted Sensory Reinnervation is an adaptation of the Targeted muscle reinnervation technique (Kuiken et al. 2007). This procedure involves denervation of the skin over the chest muscles, which is then reinnervated by the afferent nerve fibers of the residual hand, regenerated through the pectoral muscle. This enables the patient to perceive all modalities of cutaneous sensations, as parts of the lost arm and hand are

mapped to the areas of the pectoral muscle. This technique involves transfer sensation and has a potential to provide useful sensory feedback (Kuiken et al 2007).

1.4.2.2 Brain Machine Interface

Brain Machine Interface (BMI) involves direct detection of motor intentions from the central nervous system, specifically the brain, which is relayed to an external electronic/robotic effector that physically functions as a substitute to the subject body. The first comprehensive study of the electroencephalography in humans made by the German physiologist Hans Berger (Berger et al. 1929) is the chief precursor to the non invasive type of BMI. External and implantable electrodes monitoring neural system electrical activity and subsequent reconstruction of functional maps of the brain were the first efforts taken in neural interfacing. Neural activity recorded from cerebral neurons and correlation of the changes in firing pattern to the EMG signals collected during specific movements (Evarts 1966) Has been used to predict characteristics of a subject's motor movement (Georgopoulos et al. 1986 and Paninski et al. 2004), delivered somatosensory stimuli (Xu et al. 1999), or a subject's position in space (Barbieri et al. 2005). The firing rate can be volitionally modulated by the subject to generate a controllable output signal that can be used for moving the cursor on the computer screen or direct a robotic arm (Wolpaw et al. 2002, Hochberg et al. 2006 and Serruya et al. 2002). BMI's provide these users with communication channels that do not depend on peripheral nerves and muscles (Wolpaw et al. 2000). However, several BMI's include a continuous risk in recording the action potentials as it requires insertion of microelectrodes into the cortex (invasiveness), that may result in neuronal loss and scar tissue formation around the electrode tip (Scwartz et al. 2006). There are also difficulties maintaining and achieving stable recordings from individual neurons, and there is high variability in neuronal behavior (Kubanek et al. 2009 and Shenoy et al. 2011). These limitations lead to the

development of peripheral neural interfacing. Figure 0.11 shows motor commands starting in the brain follow a downstream path towards ventral spinal cord that enables in prosthetic arm control. On the other hand, sensory signals from the robotic arm take the opposite path to alert user through selective electrical stimulation of the amputated nerve. Stimulus path involves spinal cord, thalamus and sensory cortex in brain for limb awareness and feedback control.

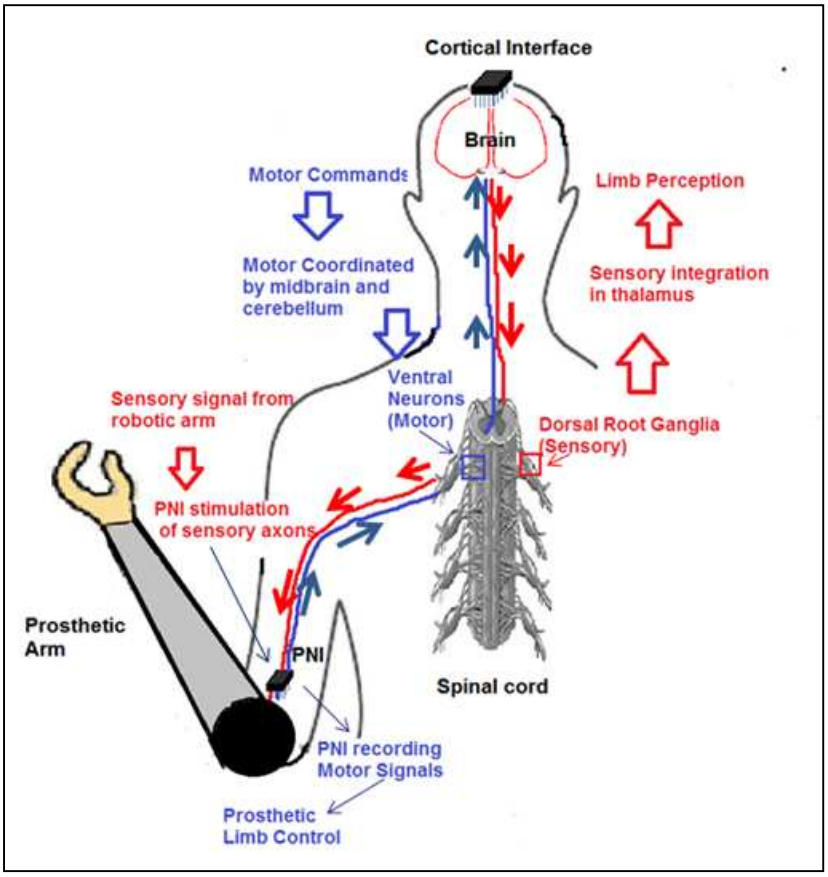

Figure 0.11: Schematic of closed loop signal processing through Cortical and Peripheral Nerve Interface

1.5 Peripheral Nerve Interfacing

Peripheral nerve interfaces (PNIs) can facilitate bidirectional flow of information i.e. record motor commands initiated by the user. In addition, sensory and proprioceptive

feedback from the limb such as movement, pressure, and temperature can be detected by sensors in the robotic arm, which is further conveyed to the user by direct stimulation of specific afferent nerve fibers at the PNI (Kim and Romero. 2012)(Figure 0.11).

Microelectrode devices that are electrically coupled to peripheral nerves or muscles are the general type of interfacing devices even if, this method involves some degree of invasiveness into the biological system (Heiduschka et al. 1998, Rutten 2002 and Navarro 2005). Current state of the art of neuroprostheses majorly addresses the development and experimental testing of interfaces to the PNS that do not damage the nerve and tissues, permit access to information from sensory afferents, selectively allow

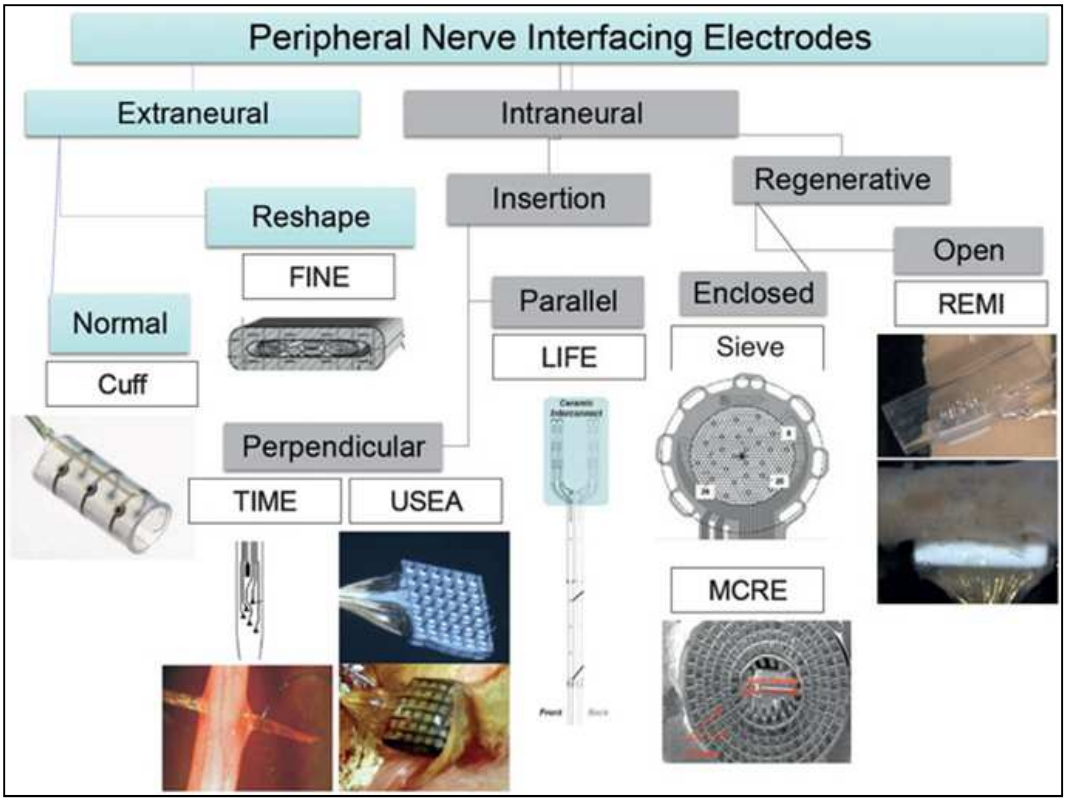

Figure 0.12: Classification of Peripheral Nerve Interfacing Electrodes (Adapted from Kim and Romero. 2012)

stimulation of multiple nerve fibers, and provide graded control of muscle force (Navarro 2005). These neural electrodes can be implanted adjacent, around or even within a peripheral nerve trunk or spinal root. Depending on the proximity to the nerve, the stimulus intensity required for activation is altered; therefore, hazardous electrochemical processes and power consumption of the stimulator system can be decreased by interfacing within the nerve stump (Loeb et al. 1996). Selective stimulation of different fascicles of axons composing the nerve may be achieved with Intraneural PNIs (Rutten 1999). However, invasiveness of nerve electrodes increases the potential to damage the nerves on which they are implanted (Lebedev et al. 2006). Therefore peripheral neural interface can be broadly categorized based on their invasiveness as compared to their selectivity into extraneural and intraneural interfaces.

1.5.1 Extraneural Interface Electrode

Cuff electrodes is a type of PNS interface electrodes, composed of an insulating silicon or polyimide tubular sheath generally wrapped around the circumference of the nerve and two or more electrode contacts on the inner surface (McNeal et al. 1985). The most common designs of cuff electrodes are ‘split-cylinder’ and ‘spiral’ cuffs (Naples et al. 1990). Selective stimulation can be achieved with accurate placement of the electrode enabling confinement of the stimulating current within a cuff electrode (Loeb et al. 1996) and can be extended to stimulation of separate axonal fascicles within the nerve, by incorporating multichannel cuff electrodes (Navarro et al. 2001). Cuff electrodes are employed to stimulate the enclosed nerve that leads to activation of efferent motor or autonomic nerve fibers. Owing to its simple interfacing mechanism, cuff electrodes can be easily implanted and the design makes it less susceptible to damage the nerve. However, during functional stimulation, cuff electrodes record multi-unitary nerve activity, causing difficulty in the identification of single spikes. Thus, the number of active axons,

the recording area and the position of active contact electrode on the cuff, limit the selectivity of neural recording.

To overcome the limitation of cuff interface, the flat interface nerve electrode (FINE) was designed by Tyler and Durand (Tyler et al. 2002) that integrated a variation in the architecture of the cuff electrode. The FINE is an extraneural electrode designed to enhance selective stimulation by reshaping peripheral nerves into a favorable geometry. The reformation of the nerve into a more elliptical shape causes easy accessibility of fascicles with central fibers relocated closer to the stimulating electrode with reference to the conventional cylindrical cuffs. The altered design enhances the interface surface area offering more contacts to be placed around the nerve for both recording and stimulation (Perez et al. 2000, Choi et al. 2001). Nevertheless, stable long-term recordings and thus the efficiency of the FINE electrodes to record and stimulate, is altered by the excessive connective tissue and epineural fibrosis growth in and around the interface (Vince et al. 2005). Despite the simple architecture and easy interface, extraneural electrodes has limited selectivity.

1.5.2 Intrafascicular Electrode (intraneural)

As the name suggests, these electrodes are placed within a peripheral nerve providing direct contact with the tissue for stimulation and/or recording; thus enhancing selectivity and signal-to-noise ratio of the neural recordings. The design facilitates the use of smaller stimulus intensities to produce comparable results with those obtained form extraneural electrodes and reduced cross-talk while stimulation of specific fascicles (Yoshida et al. 2000). The immense selectivity of intraneural electrodes, as compared to extraneural, has assisted researchers to understand how individual sensory receptors characterize cutaneous sensation, heat, pain, and proprioception as trains of action

potentials. Flexible intrafascicular electrodes may involve the use of silicon-, polyimide-based substrates or intrinsically conductive fibers.

Intrafascicular electrodes may be differentiated based on the insertion direction. Longitudinally implanted intrafascicular electrodes (LIFEs) are 25μm Pt/Ir insulated conducting wires metalized Kevlar fibers, used to interface with constrained group of axons within nerve fascicle (McNaughton et al. 1996, Yoshida et al. 2000). Also electrical stimulation through the implanted electrodes induced graded sensations of touch, joint movement, and position, referring to the missing limb. The transverse intrafascicular multichannel electrode (TIME) is a hybrid of the LIFE electrode (Boretius et al. 2010). This electrode is implanted into the nerve transversally, thereby allowing easy access to different subsets of nerve fibers. Similar to LIFE, these electrodes also provide good contact with several fascicles in a nerve cross-section with reasonable spatial selectivity. Even though LIFE and TIME provides excellent selectivity, implantation of these electrodes in multiple fascicles and selective stimulation of fiber bundles to the appropriate muscle groups is still a challenge.

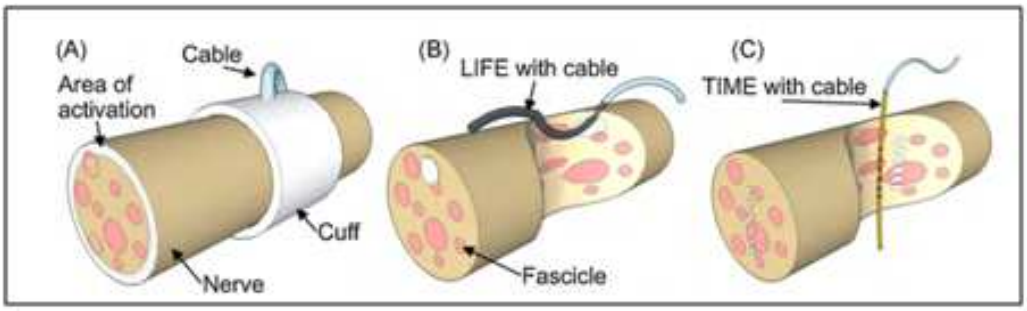

Figure 0.13: Schematic depicting techniques of peripheral nerve interfaces with predicted areas of activation during electrical stimulation (hatched area) with one implanted device. (A) Cuff electrodes (B) LIFEs (longitudinal intrafascicular nerve electrodes (C) TIMEs (transversal intrafascicular multichannel electrodes (Boretius et al. 2010)

Researchers in the University of Utah (Branner et al. 2000) designed a slanted 100-electrode microelectrode array incorporating the selectivity of the intraneural

electrode and the ease of implantation, stability, and biocompatibility of the extraneural electrode. The UTAH electrode array is the penetrating type of intrafascicular peripheral nerve interface that employs insertion of the MEA into the intact nerve for recording and/or stimulation. This electrode array is capable of recording single units from approximately 50 electrodes at an instance and electrical depolarization was able to selectively evoke graded recruitment of force in muscles (Branner et al. 2000). The use of this electrode interface in peripheral nervous system involves significant challenges like mechanical damage of the nerve during insertion causing axonal compression and formation of neuromas (Branner et al. 2004). Moreover, electrode inflexibility, electrode breakage and micromotions result in secondary injuries amplifying the inflammatory response (Gonzalez et al. 1997), thus altering spike amplitude (Merrill et al. 2005).

1.5.3 Regenerative Nerve Interface

The peripheral nerve is uniquely capable of spontaneous recovery from injury by regenerating the lost connections, unlike the central nervous system (Burnett et al. 2004). Post severe peripheral nerve injury the distal portion suffers a series of histological alterations that include Wallerian degeneration involves physical fragmentation of both axons and myelin followed by the myelin debris phagocytosed by proliferating macrophages and Schwann cells creating a mitogenic medium for Schwann cells (Fawcett et al. 1990, Burnett et al. 2004). This leads to the expression of various regeneration associated proteins like laminin, fibronectin, cytokines and neurotrophins thus enhancing rate of axonal regeneration, neuron growth and their reinnervation to their targets (Schmidt et al. 2003).

Thus the regenerative nerve electrodes are designed to interface with a large number of nerve fibers and implantation between the transected stumps of peripheral nerve. One of the first developed regenerative interface, Sieve electrodes are

strategically positioned around the array holes so as to maximize contact with the regenerating nerve fibers (Dario et al. 1998) thus aiding optimal recording of action potentials and stimulation of individual axons or small fascicles. These electrodes provide a physical barrier to regeneration limiting the elongation of a few sub-types of regenerating axons depending on size of via holes (Navarro et al. 2005, Navarro et al. 1996).On the contrary, the efficiency of regenerative electrode relies on factors like, the success of axonal regeneration through the perforation of the sieve, nerve damage due to mechanical load of electrode or constrictive forces within the holes, and the biocompatibility of the interface material (Navarro et al. 1996, Heiduschka et al. 1998).

In order to overcome this drawback, the Regenerative Multi-Electrode Interface (REMI) was designed to provide a non-restrictive path for the regenerating axons (Garde et al. 2009). This regenerative type interface consists of a collagen-filled tube with a functional Floating multi-electrode array (FMA) to allow the axons grow transversely to the needle electrode array. This architecture predominantly reduces restrictive axonopathy and facilitates selective stimulation of different neuron types and sensory feedback (Lotfi et al. 2011).

1.5.4 Limitations

With the numerous strategies developed in PNIs to enhance volitional control of prosthesis as described, regenerative type of PNIs is most selective but involving high degree of invasiveness. The current state of the art of neural prosthetics is aimed at maximizing comfort and ease of use, with increased degree of freedom. However, these methods seem to experience several limitations that fall in the following categories:

1.5.4.1 Selective electrical stimulation of peripheral nerve fibers versus Invasiveness

Selectivity is defined as the capacity to stimulate one population of neurons without simultaneous activation of another, often neighboring population of neurons.

However, equilibrium must be attained between the density of the signal and the extent to which delicate physiological structures can endure the interference of the interfacing device (Grill et al. 2010). In peripheral nervous system, interfacing involves multiple fascicles with a certain degree of mixed motor-sensory axon modalities in each fascicle (Stewart et al. 2003) and in case of the regenerative peripheral interfaces, motor and sensory axon mixing increases due to regeneration (Brushart et al.1995). Thus recording exclusively from motor axons and selective stimulation of specific sensory modalities from a mixed nerve is an added challenge. The difficulty in selectivity arises from the fundamental property of nerve fiber stimulation i.e. the current required for extracellular stimulation of axons which depends on the distance between the electrode and the nerve fiber, and the diameter of the nerve fiber itself (McNeal et al. 1976). Durand and Lertmanorat had identified that, large myelinated axons (e.g. Aα fibers) are depolarized with smaller currents, while smaller diameter neurons (e.g. C fibers) require larger stimuli (Durand et al. 2004). Therefore, using cuff electrodes for stimulating small caliber fibers will stimulate large size axons also. Nevertheless, increasing selectivity results in an increase in invasiveness. The use of penetrating electrodes and its mechanical mismatch with the tissue, cause severe inflammation and aggravated foreign-body response. (Zhong et al. 2001)

1.5.4.2 Recording sensory information for control and feedback

In most cases, amputation results in nerve stumps with no distal targets. These residual nerves when redirected have shown to translate their inherent function (motor/ sensory) in the re-innervated region. Thus, tapping the persistent neural activity from the residual nerves would not only provide the efferent command signals for prosthetic control but also effective afferent sensory feedback system. On the other hand, the residual distal nerve stump following limb amputation may provide command signals from

motor nerve fibers for prosthetic control. Studies have shown that in the absence of visual input, electrical stimulation of transected peripheral nerve in amputees can enable them to judge grip force and joint position in an artificial arm (Dhillon et al. 2005).

1.6 Extracellular Electrophysiology

The fundamental unit of information in the nervous system is the action potential generated by a neuron. The firing frequency of neuron ranges from zero to hundreds per second, facilitating efficient encoding of information over a broad dynamic range. The classical representation of an action potential generation initiates with a neuron at rest. There are primarily, three simultaneously active currents responsible for an action potential (AP); the 3 phases of the AP correspond to the current that is dominant at that time. Thus, the initial brief positive peak of the spike shape is attributed to the positive capacitive current; followed by the main negative peak is caused due to the influx of Na+ ion current driving the action potential; and subsequently the final positive phase accredited to the repolarizing K+ ion current flowing out of the cell. A single neuron follows the law of all-or-none to fire an action potential, i.e. any stimulus with intensity above the neuron threshold is capable of evoking a spike.

On the contrary, the compound action potential of a nerve is graded in nature. Action potentials generated from neighboring neurons cause the release of neurotransmitters that will result in either excitatory or inhibitory actions. Activity of a neuron is controlled by combined effect of all passive synaptic inputs and an action potential is generated when there is an adequately large net excitation.

The source of the signal recorded via an electrode placed near an active neuron within the tissue is the trans-membrane current that is conducted during the action potential. The electrical potential in the extracellular space is summation of shifted (in space and time) membrane currents originating from all active nerve fibers in during the

propagation of an action potential. The average resting potential of mammalian neurons is approximately −60 mV, and intracellular voltages reach the positive mV range during an action potential (Kandel et al. 2000, Cox et al. 2008), but extracellular signal voltages are much lower (Struijk et al. 1999); for instance, regenerative electrodes measure signals ranging to several hundred microvolts (Edell et al. 1986, Bradley et al. 1997). Therefore, in addition to the low amplitude voltages, neural signals recorded in close proximity to contracting muscles may get contaminated by electromyogram (Branner et al. 2004) or by electrical artifacts present during electrical stimulation. Furthermore, due to the linear relationship of signal amplitude and fiber size, the largest axons provide the dominant signal in multi-unit recordings (Marks et al. 1976).

Neuronal firing pattern may be influenced by the intrinsic electrical properties (regulation of voltage-dependent ion channels can modulate a neuron's electrical properties) of the neuron or by the presence of fast synaptic potentials, acting on the millisecond timescale. Some neurons can also generate action potentials spontaneously, in the absence of synaptic inputs. Figure 0.14, schematically represents the variety of neuronal firing patterns that can be observed, even in the absence of synaptic inputs. Example: Some neurons maintain a stable resting potential ('a' in Figure 0.14), but others may fire repetitively (b), randomly (c), or in bursts (d). (Jones 2001)

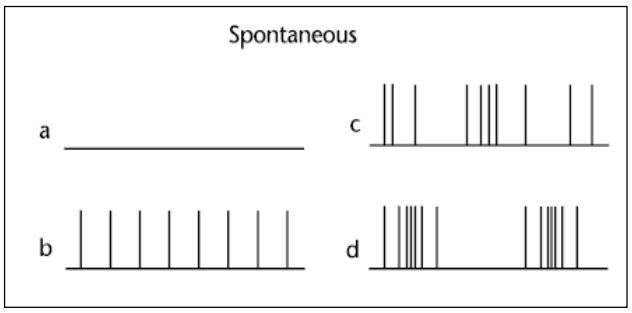

Figure 0.14: Schematic illustration of some possible neuronal firing patterns. Action potentials are simple vertical lines, and sub-threshold changes in voltage are not shown. a) Stable resting potential b) repetitive c) random d) bursts

On the other hand, several studies have demonstrated that there is heterogeneity in the soma spike shape of sensory neurons (Görke et al 1980, Harper et al 1985, Yoshida 1978) with distinct relationship between action potential shape and receptor modality (Gee et al 1999). However, no relationship has been demonstrated between sensory modalities and spike shapes of action potential recorded from a mixed nerve. Each neuron fires action potentials of a particular shape, based primarily on the morphology of its dendritic tree, its position and orientation relative to the recording electrode, the distribution of ionic channels and the non-homogeneity of the extracellular medium (Gold et al. 2006, Quiroga 2009). As an action potential is fired within a neuron, ion-channels on its membrane open and the resultant electric current due to the ions flowing through them together with the resistive extracellular volume around the neuron generates local changes in extracellular voltage that can be sensed with a recording electrode.

A typical extracellular potential has a large extracellular negative wave representing the net inward current flow during the depolarizing portion of the intracellular action potential and the extracellular late positive wave corresponds to the net outward currents during the repolarization and after-hyperpolarization of the intracellular action potential (Henze et al 2000). Figure 0.15 shows that the extracellular potential shape qualitatively matches the second time derivative of the intracellular potential (Cohen et al 2000).

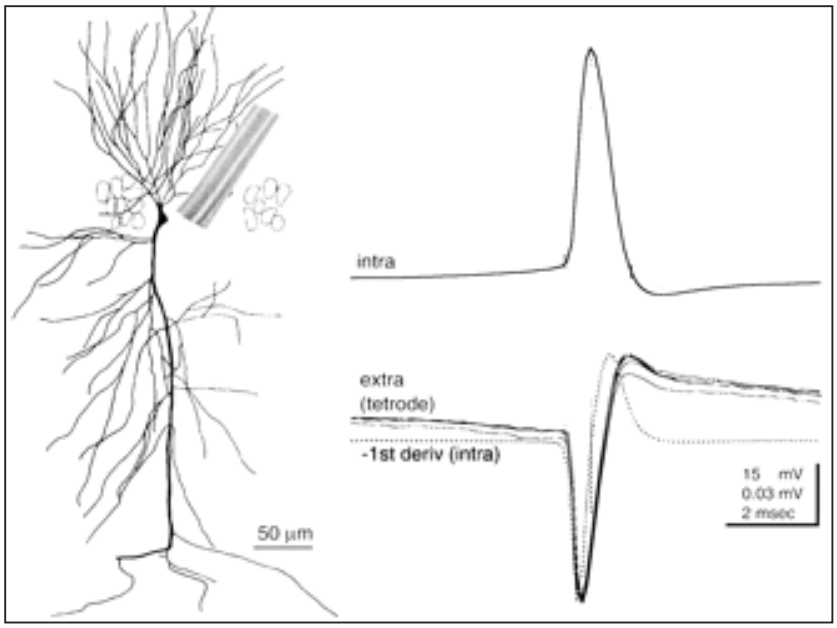

Figure 0.15: Shows the average intracellular action potential (intra) and extracellular spike recorded from the neuron relatively a good match to 1st derivative approximation of Intracellular AP (Adapted from Henze et al. 2000)

1.6.1 Stretching Physiology

Natural physiological conditions imposed during posture and movement expose nerves to various mechanical stresses (Figure 0.16). Tensile stress may act on tissues either along or at right angles to the length of the nerve, resulting in longitudinal or transverse stress in the nerve respectively. During a joint motion, the nerve is naturally under tensile stress and adapts to it by both elongating and gliding (Millesi et al 1995). This phenomenon is induced in an animal model as cyclic limb stretching for this experimental design. Mechanical stretching is identified to cause morphologic and functional changes in peripheral nerve (Kwan et al 1992). Several groups have reported that stretch can damage the myelin (Abe et al. 2002) as well as the cytoskeleton (Jafari et al. 1998, Maxwell et al. 1996).

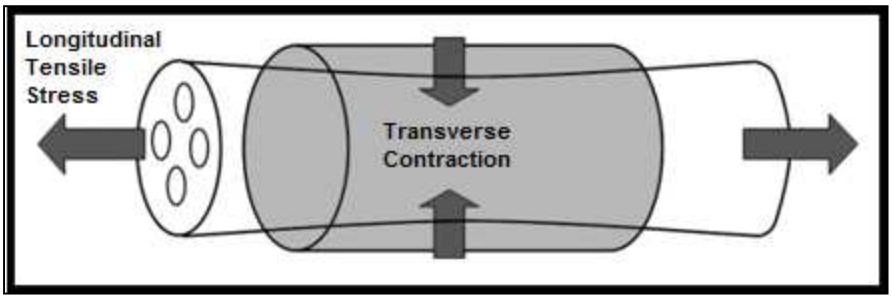

Figure 0.16: Physical stresses exerted on the peripheral nerve. (Adapted from Topp et al. 2006)

1.7 Specific Aims

Although, several studies have theoretically proved the feasibility of applying Peripheral nerve interfaces (PNI) for motor control and sensory feedback in prosthetics, the practicality of attaining specific motor commands to control the robotic prosthetic limb and stimulating definite sensory axons specific to each of the sensory modalities such as thermoception, mechanoception or proprioception, has not been established. In this study, the regenerative multi-electrode interface (REMI) is used to record the neural activity specific for sensory sub modalities.

Specific Aim 1: To determine if firing rate, amplitude and shape of single unit spikes can be used to distinguish between sensory sub-modalities in the regenerated sciatic nerve of a freely moving Rat.

Specific Aim 2: To test the stability of waveforms before and after cyclic stretching of the injured limb and identify any specific subset of single unit spike waveforms are elicited by cyclic stretching.

Chapter 2

Materials and Methods

2.1 Regenerative Multielectrode Array and Conduit Assembly

Regenerative Multi Electrode Interface has an open architecture consisting of a Floating Microelectrode Array (FMA) encompassed by a polyurethane tube. Each FMA has 18 platinum/iridium micro wire electrodes coated by Parylene-C for insulation with impedances at 1 KHz ranging between 150KΩ - 250KΩ (Microprobes Inc., MD). Electrodes were positioned in a 5-4-5-4 pattern with a regular inter-electrode spacing of 400 μm (Figure 2.1A) so as to enhance contact with the regenerating axons. Each electrode shaft was customized such that it tapered from a 50μm diameter at the base to a sharp tip and length varied between 0.7 and 1.0 mm (Figure 2.1B). 18 such electrodes were housed on to an alumina ceramic base plate, 250μm thick, which is encapsulated within a 5mm long and 3mm wide, polyurethane guide tube thus forming the REMI (Figure 2.1C) (Micro Renathane®, Braintree Scientific Inc.).

This base plate is connected via 4.5 cm gold wire to an 18-pin omnetics connector sealed with epoxy within a Titanium pedestal (Figure 2.1D) to prevent moisture and possible debris exposure. The connecting cable is made of multiple 25 μm gold wires helically intertwined to maximize flexibility and strength, and insulated by Parylene-C followed by a thin coat of NuSil-type non-restrictive silicone elastomer for improved biocompatibility. The custom-made titanium pedestal was designed to have two base flanges to assist attachment to the pelvic bone and a removable lid fastened with screws. Preceding implantation, the assembly was sterilized with pure ethanol followed by overnight exposure to UV light and tube lumen was filled with collagen (polymerized at 37ºC) from Chemicon, Temecula, CA.

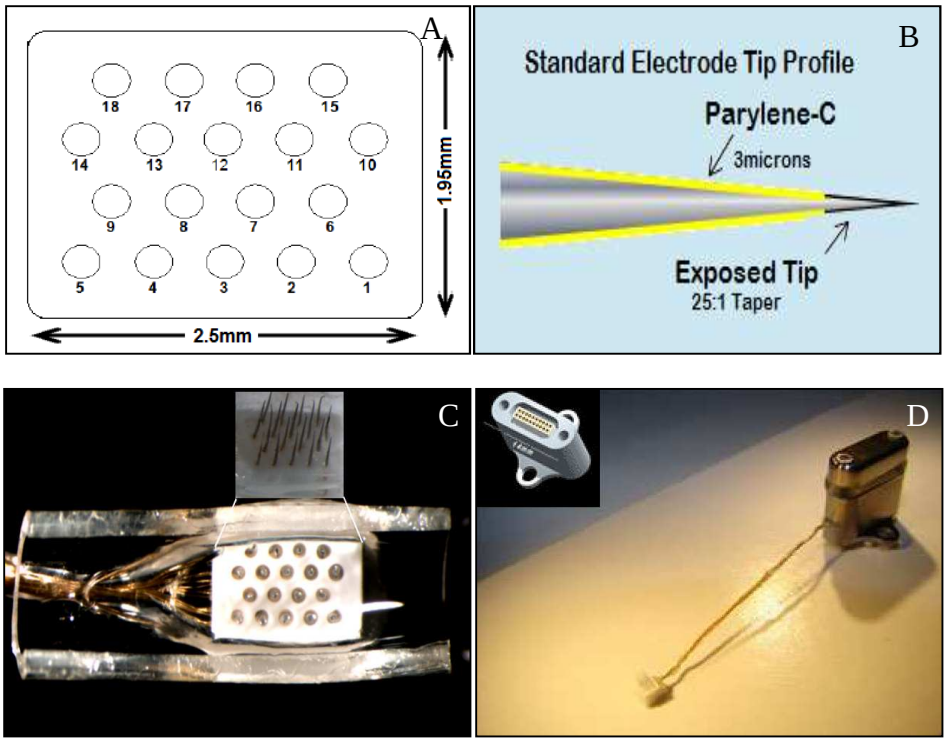

Figure 2.1: Shows (A) Arrangement of 18 electrodes with dimensions of the Floating Multielectrode array as in REMI design (Array dimensions 2.5mmX1.95mm)(*Courtesy* Microprobes Inc., MD), (B) A standard electrode tip profile with Parylene-C insulation, (C) FMA encased within a Polyurethane tube (enlarged view of electrodes), (D) Titanium pedestal housing Omnetics connector with array with the pedestal schematic (*Courtesy* Microprobes Inc., MD)

2.2 Animal Preparation and Surgical Implantation

The experiment involved a total of 22 adult lewis rats, each weighing between 215 - 275gm. The rats were anesthetized by inhaling Isoflurane of 5% concentration in 100% Oxygen and maintained at a reduced 2-2.5% Isoflurane in 100% Oxygen. Isoflurane was used as it has minimal impact on nerve conduction velocity and recent study suggests that it is the safest, most effective method of anesthesia for murine animals models (Oh et al. 2010). Anesthetization protocol during the entire study did not involve the use of nitrogen gas. Eyes were kept hydrated with ophthalmic ointment and body temperature was monitored throughout the surgery. Prior to implantation the dorsal

side of the pelvis and the left thigh regions were shaved and cleaned using 70% Isopropyl Alcohol and Povidine-iodine for disinfection. An incision was made vertically along the sacral line over the pelvic region. The muscle and fascia around the spine was cleared, the tips of the dorsal processes were clipped and the exposed pelvic area was cleaned and dried. The percutaneous titanium pedestal was then affixed to the pelvic bone using bone cement (Biomet; Warsaw, Indiana, USA). A second incision was made on the left leg succeeded by parting of overlying muscles and fascia to expose the underlying Sciatic nerve. The gold connecting cable with the array is passed subcutaneously to the second incision site. The sciatic nerve was transected just before the branching and the distal and proximal nerve stumps were inserted into opposite ends of the tube and sutured in place with monofilament suture for end-to-end repair. The fascia and skin was then sutured in layers using resorbable (6-0 chromic gut) and surgical staples respectively. Post-operative care involved topical application of antibiotic ointment (Fougera, Triple antibiotic Ointment) at the surgical site followed by intra-muscular injections of antibiotic (Cefazolin, 5 mg/kg, IM) on the thigh and pain control injections (Buprenorphine, 0.1 mg/kg, SC) subcutaneously. Post-surgery, animals were maintained in humidity/temperature controlled room with 12 hour light/dark cycle with regular supply for animal feed and water. All the surgical procedures, including pre- and post animal care were performed in agreement to the guidelines of Institutional Animal Care and Use Committee (IACUC) of University of Texas at Arlington.

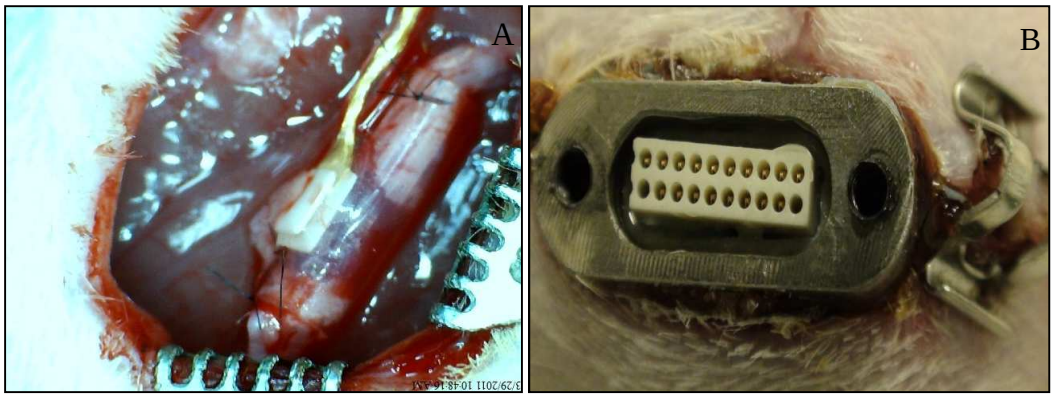

Figure 2.2: Representative photographs of A) The proximal and distal ends of transected sciatic nerve sutured to the polyurethane tube mounted with the REMI electrode array. B) Titanium Pedestal housing the Omnetics connector that is mounted on the pelvic bone

2.3 Electrophysiological Recording

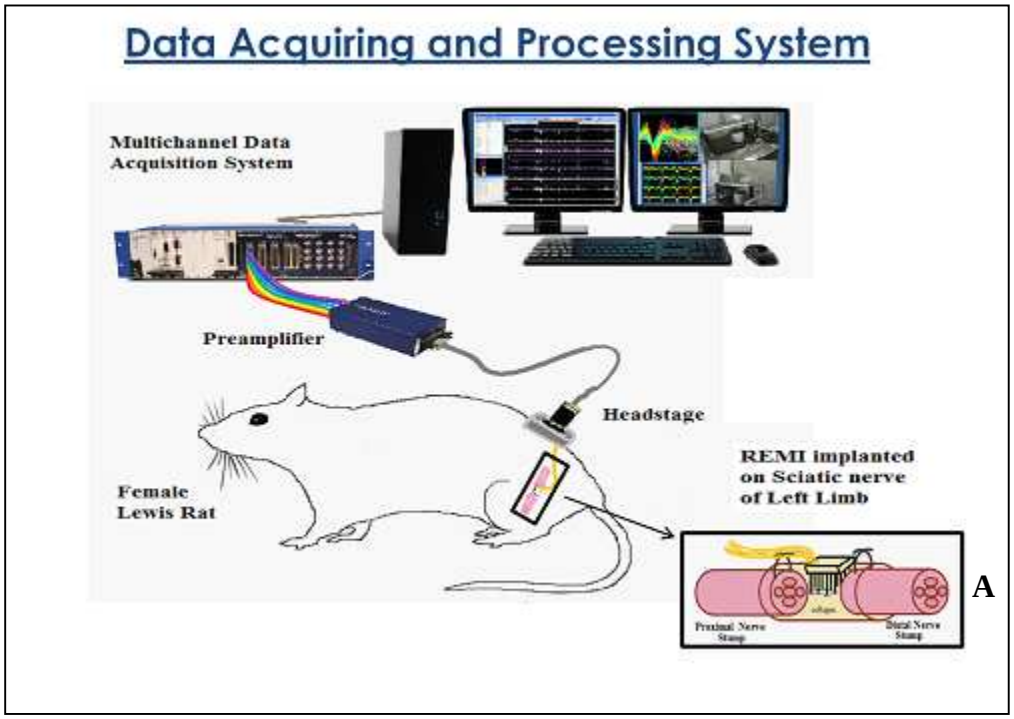

Figure 2.3: Schematic representation of the recording setup. REMI implanted into the left hind limb of the animal with insulated wires running subcutaneously to connect the electrode array to the connector in the pedestal. External wires connecting head-stage, amplifier-box and ultimately to the Omniplex Multichannel data acquisition chassis and the computer. (A) Magnified view of the interface with the nerve sutured to the guide tube

Wideband neural activity of regenerating axons in a freely moving rat was acquired weekly using the Omniplex Multichannel Data Acquisition system (Plexon Inc., USA) with synchronized live video recording by Cineplex digital recording and tracking system (Plexon Inc., USA) . The acquisition system was equipped to record from 16-channels, at an accuracy of 25 seconds. The recordings were obtained at as early as 7 days post implantation and extended till 42 days. A typical recording session involves brief animal anesthetization of 1-2 minutes approx. (3% Isoflurane in 100% Oxygen) for removing the titanium pedestal lid and attaching a headstage (Op-amp based, unity-gain) to connect to the 20x pre-amplifier box via an Omnetics connecter cable. The electrical grounding was done by connecting wires from one of the pedestal screws, pre-amplifier and the Faraday Cage (site of recording setup). The animal was then let to regain consciousness and stabilize before the neural data acquisition. The signals were routed to the Omniplex chassis via a ribbon cable, for further amplification and digitization. The amplifier was characterized by its high signal-to-noise ratio (SNR), good common-mode rejection ratio (CMRR) at 0-60 Hz (>100 dB), programmable reference channel, programmable gain from 250X to 8000X gain and 4-pole Bessel analog high-cut filter at 8 kHz. The chassis was then connected to a computer to allow real-time monitoring of neural signals and tuning of parameters while recording. All the neural signals were typically recorded with a gain set at 8000X during the different behavioral tests. The animal was again briefly anesthetized post recording, to disconnect the headstage and then returned to its cage.

2.4 Behavioral Tests

The entire study involved acquisition of neural data in response to several sensory modalities. After the animal was prepared for recording and placed in the faraday cage, neural activity was recorded for time duration of 300 seconds while the animal was

allowed to move freely without any specific stimulation (awake resting). This was followed by several behavioral tests to evaluate functional recovery.

2.4.1 Nociceptive Recovery

The acute axotomized animals were assessed for nociceptive recovery by eliciting pain response to thermal stimulation by means of the Ugo Basile Plantar device (Ugo Basile, Varese, Italy). Animals were initially allowed to stabilize in a plexiglass chamber before conducting the test. The Ugo Basile Plantar device, an infra-red radiant beam was applied to the plantar surface of hind paw and a photocell (7370-372EW01) detects time duration starting from the instance of stimulus application to the time of paw withdrawal and or paw licking, called paw withdrawal latency period. The device was programmed to a precision of 0.1sec so as to reach 55^0C in approximately 12 second (Plantar test manual, UGO Basile biological research apparatus). The next trial was recorded after 10min to the first recording so as to avoid response due to anticipation (Romero et al. 2007).

2.4.2 Tactile Perception Recovery

The Mechanoceptive sub-modality was evaluated by the animal response to the application of force onto the plantar surface of the paw using Plantar Von Frey filament of the anesthesiometer. The device was equipped to exert a gradual increasing force of 0.5 g steps within 20 seconds up to a maximum of 50 g via a 0.5mm diameter needle like filament (UgoBasile 2012). Force and the response time for paw withdrawal were registered. Multiple trials were done with 10 min intervals.

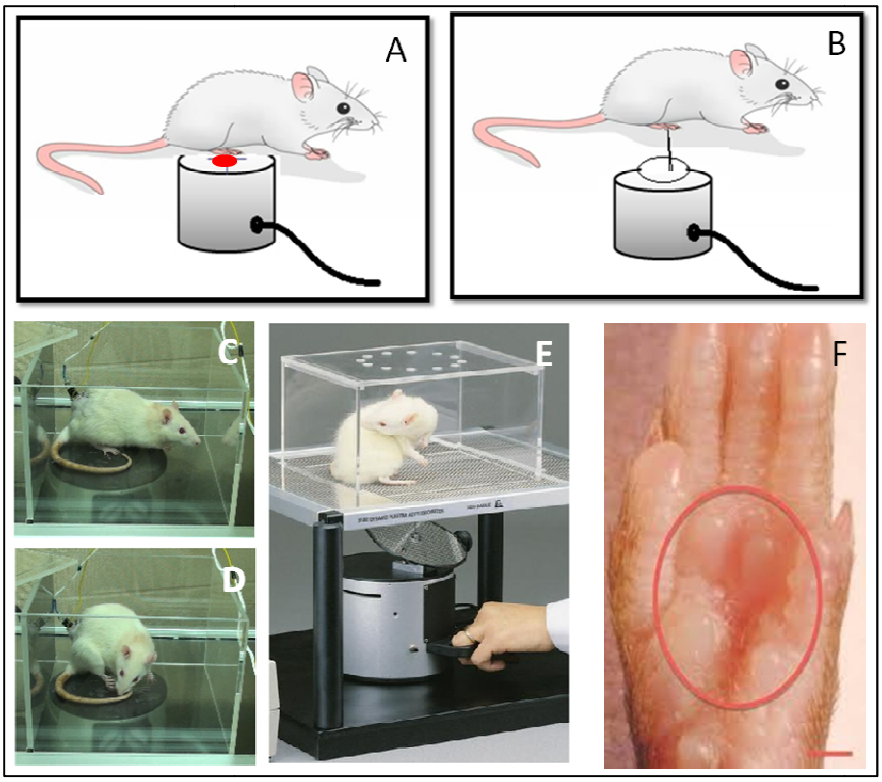

Figure 2.4: Schematic showing behavioral tests A) Thermal stimulus via infrared beam (Ugo Basile Plantar Device) B) Mechanical stimulus via Plantar Vonfrey Filament C) and E) Experimental setup for the behavioral tests (Courtesy UGO Basile) D) Paw withdrawal and Paw licking at response to the stimulus F) Area of Receptive Field for stimulation

2.4.3 Stretching

These electrophysiological recordings were performed weekly upon a separate group of animals that were subjected to different degrees of periodic cyclical limb stretching, for a maximum of 30 days, beginning from 7 days post-implantation. This experimental paradigm involved 2 sub groups of animals each being subjected to 70% (moderate limb extension) or 100% (extreme limb extension) stretching. A typical limb stretching session was achieved using a custom-built device, operated via Lab VIEW script, involving a computer controlled linear actuator that drives a clamp along two stationary rails (Figure 2.5) for approximately 130 cycles. The clamp clasps the paw of

the rat and the device was programmed to stretch the limb from a relaxed position to either 70% or 100% of full limb extension. The animal was immobilized by fixing the pelvis with the help of 2 rods as shown in the Figure 2.5. For a typical experimental setup, initial calibration is done when the animal is positioned such that position 1 is set in the actuator controls when the thigh is at 90° to the pelvis; and position 2 is set when the leg is fully extended and is considered to be a stretch of 100% (excessive stretch). The actuator is then set to cycle between Position 1 and 70% of Position 2(normal stretch) for 10 minutes at 20 mm/sec.

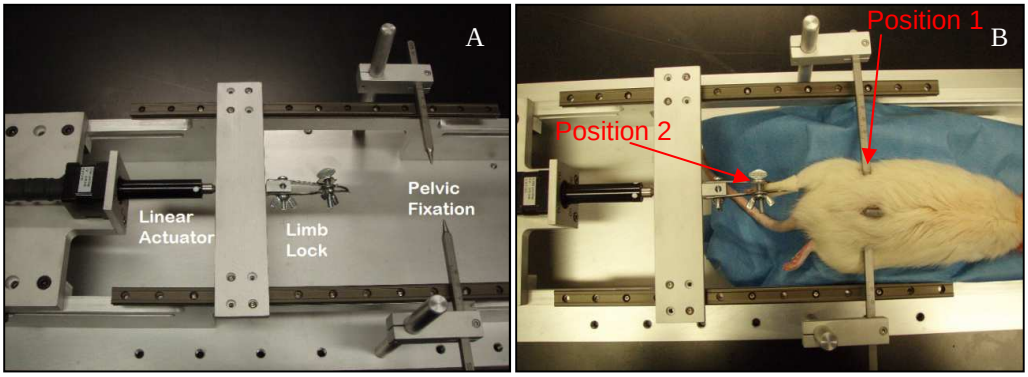

Figure 2.5: A) The Computer Controlled Mechanical Device for Cycling Stretching of Hind Legs. B) Position 1 showing pelvic fixation and Position 2 showing clamped paw for cycling stretching in the caudal direction

Then the animals were subjected to the limb stretching session under the state of anesthesia (continuous inhalation of 2% isoflurane in oxygen) for 10mins (duty cycle = 1/13) and subsequent 5 minute long recording session after the animal is completely recovered and stabilized. The maximum length of stretching the limb is subjective to each animal and ranges between 30-45 mm from the pelvic fixation. The animal was then re-anesthetized to allow for disconnection of the recording equipment. The total time in between the pre-stretch recording session and the post-stretch recording session was typically about 30 minutes.

2.5 Data Analysis

2.5.1 Sorting

The continuous wideband raw neural recordings were processed using Offline Spike Sorter (Plexon Inc., USA) to sort the spikes. Offline sorter operates on the principle of Logarithmic histogram of peak heights for waveform detection; and three-component Principal Component Analysis (PCA) to isolate the Single Unit Spikes (SUS) from the noise and the other neural signals (Chapin et al. 2004). Initially data from all the 16 channels were filtered using an 8-pole Bessel high-pass filter at 300Hz (Moiseenkova et al. 2002, Gire et al. 2008) so as to remove the low-frequency motion artifacts and power line interference (Logothetis 2002) and the neural activity is composed of multiple frequency components, such as Single-unit activity and Multi-unit activity fall in the range of 300-6000 Hz whereas Local Field Potentials is the low frequency activity ranging between 8 to 200 Hz (Mattia et al. 2010). The SUS waveforms are detected based on peak detection (first local maxima after sort start) with selected threshold crossing of -4.5 sigma noise level, employed on the amplitude of the filtered signal illustrated as solid red line in Figure 2.6A. The length of extracted waveforms was 2500μsec (i.e. 100 samples) and all the waveforms were aligned with the pre-threshold period set at 500μsec. In Offline Spike Sorter these detected waveforms, associated to individual or group of neurons, are classified by PCA and projected in orthogonal planes as a 3D spatial distribution, and each group of SUS is represented as a PCA separated cluster using waveform contouring method Figure 2.6C. The action potential waveforms can be detected from the histogram of logarithm of peak heights with dashed white line indicating zero, and dashed blue lines indicating the 3 sigma noise levels. The filtered signal lies in the frequency range of 300 Hz to 8 kHz and waveforms are identified based on the spike amplitude threshold of above the -4.5 sigma noise level.

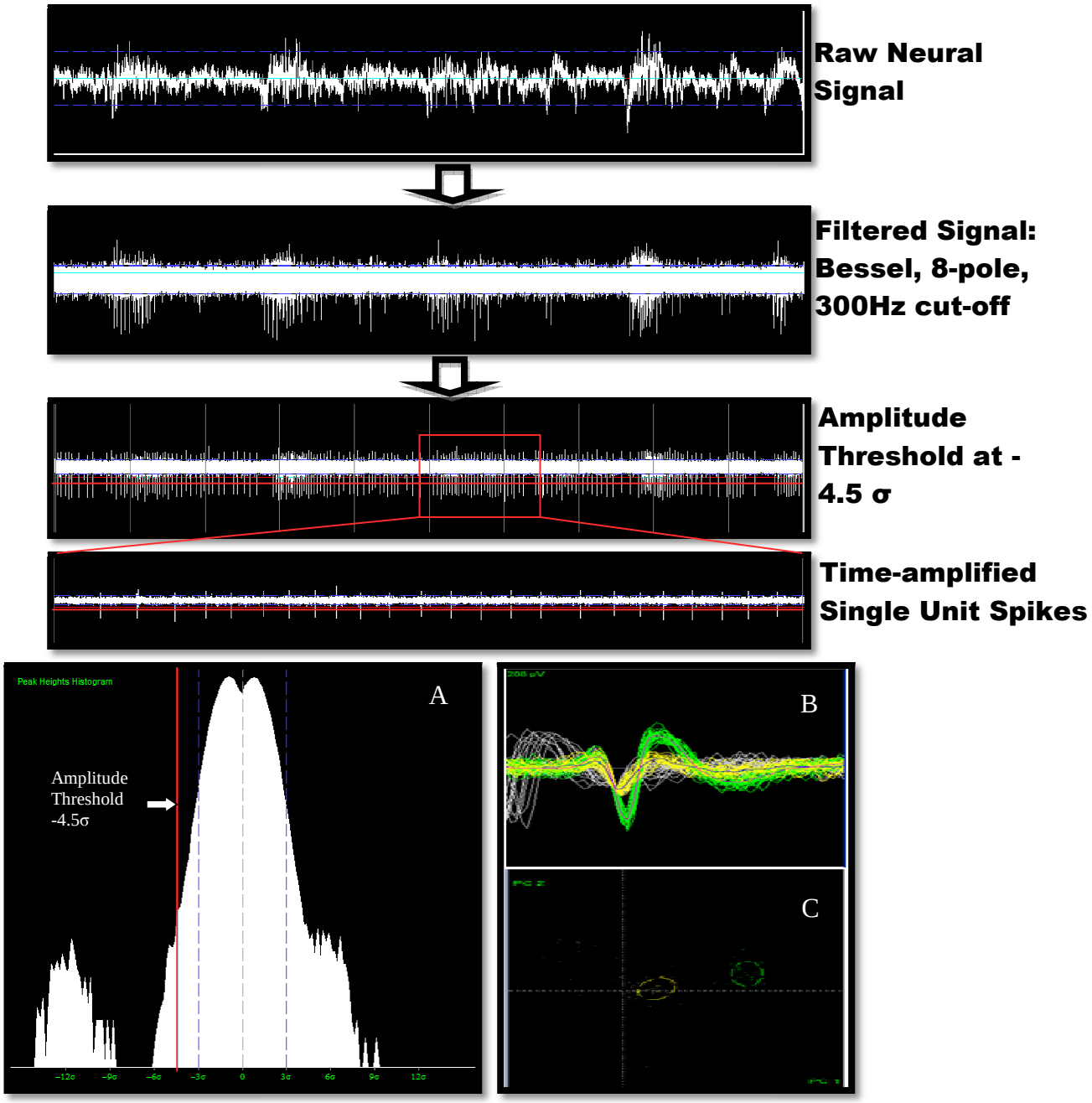

Figure 2.6: Steps adapted for sorting of spikes from Raw neural signal. A) Histogram of peaks with red line indicating the threshold level. B) Two distinct Single Unit Spike waveforms with background noise C) Projection of Isolated unit PCA clusters

2.5.2 Extraction of Parameters

A MATLAB program has been written to extract sorted waveforms from .plx files and return some of the important parameters associated with the waveforms. The first part of the program outputs average peak-to-peak voltage, average firing rate, mean inter-spike interval, median inter-spike interval and depolarization time of the average waveforms. The second part of the program yields some of the wave shape parameters such as time differences between zero crossings (base line crossing) of the wave and Elevation of the peaks with respect to the zero crossing line.

An interactive program is written for the user to select the .plx file to be analyzed and the program processes the information present in this file and exports all the statistics on the waveforms to a Microsoft Excel file. For example, if the signal to be analyzed is '3a' in case of rat R69, the user is prompted to first select the corresponding .plx file and then input these values interactively. Additionally, the user is asked to enter the day and style of recording. A function 'plx_waves_v' imports the waveform data from raw file (.plx) as shown in the Figure 2.7A to a MATLAB readable attribute called 'wave'. This 'wave' constitutes of X and Y coordinates of all the sorted waveforms where X coordinate represents the voltage and Y coordinate represents the timestamps corresponding to each voltage. This 'wave' is plotted in MATLAB as an output and is shown in the Figure 2.7B. To calculate average waveform (avg_wave), 'mean' function in MATLAB is used. This is represented by Figure 2.7C. Peak to peak voltage (Vpp) is calculated by finding the difference between maximum and minimum voltages of the average waveform. In the next step mean interspike interval (ISI) and median ISI are calculated based on the difference between consecutive timestamps.

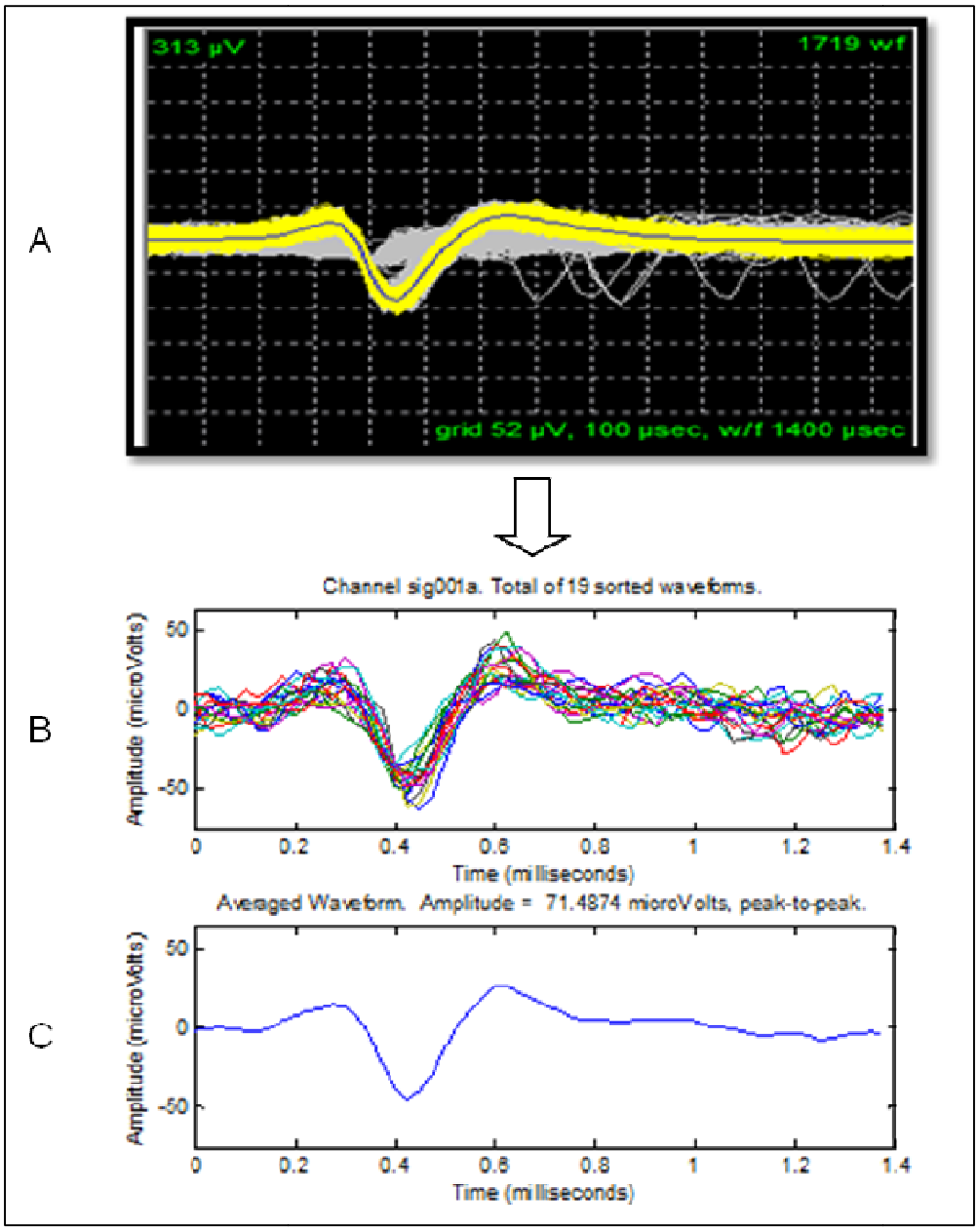

Figure 2.7: Transformation of raw Wave Form data into MATLAB format

'Depolarization time' of the average waveform is calculated by traversing reverse as shown in the Figure 2.8 from trough (minimum point) of the 'avg_wave' curve to the

previous highest peak of the curve. The time difference between these two points is calculated to get the depolarization time.

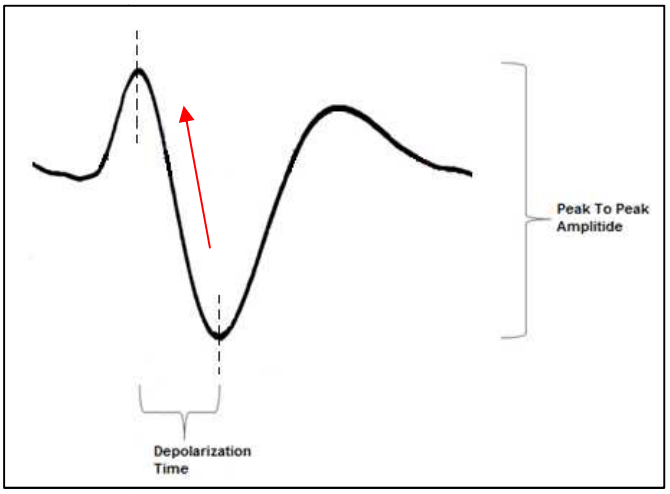

Figure 2.8: Representation of Action Potential depicting Depolarization Time and Peak-Peak Amplitude

In the next part of the program, wave shape parameters are calculated. During the intermediate step of this part of the program, different parameters were considered to analyze the wave shape. One such parameter was the angle between the “best fit line from first peak point ‘1’ to the minimum point ‘2’ on the curve” and the “best fit line from the minimum point ‘2’ and next highest peak ‘3’ on the curve” (Figure 2.9). To find this parameter, the first step was to find the best fitting curve and different approaches were used to find the best linear approximation.

Method 1: This is the basic linear curve fitting technique with two end points and a straight line joining them. This, however, had a significant deflection from the actual curve as shown in the Figure 2.9.

Method 2: This is the least mean square error based method which is the most commonly used curve fitting technique. The ‘fit’ function in MATLAB, by default, implements this technique. This technique minimizes the root mean square error

(RMSE). For instance, if θ is the estimated parameter and θ' is the estimator, then $MSE(\theta') = Avg(\theta' - \theta)^2$.

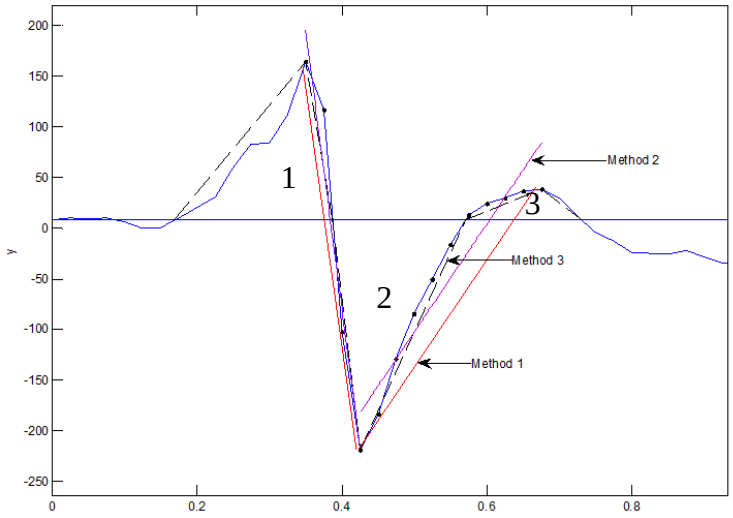

Figure 2.9: Different Types of Linear Curve Fitting Approaches

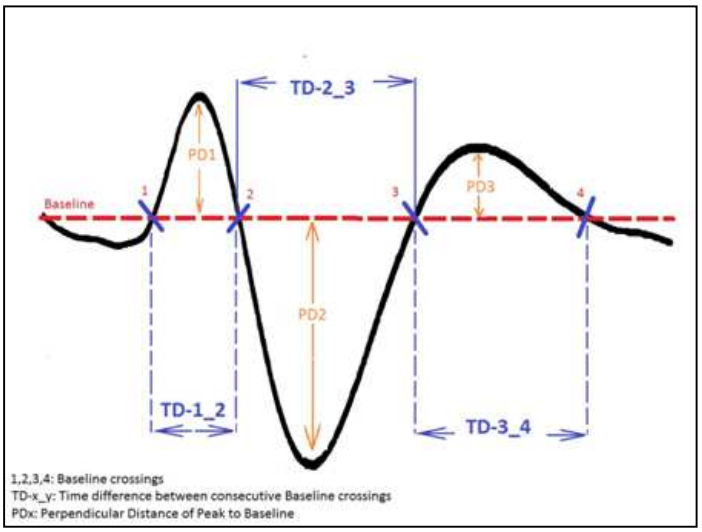

Figure 2.10: Wave Shape Parameters of a Typical Action Potential Curve

Although Method 2 was the best technique to find the angle between the lines, the above methods were not considered as it was decided that only angle parameter was

not suitable for wave shape analysis and Method 3 gave a more accurate linear representation of the wave shape.

In the final step of the program, an alternate approach was used to analyze the wave shape. The idea here is to detect the peaks and baseline crossing coordinates. The baseline is a horizontal line drawn from the starting point of the wave. In Figure 2.10, this is represented by red dashed line. Thus coordinates for zero crossing points 1, 2, 3 and 4 as shown in the figure were found. The first three wave shape parameters are determined by calculating time difference between consecutive zero crossing points shown as TD-1_2, TD-2_3 and TD-3_4. The next three parameters are the elevation of the peaks (maximum and minimum) with respect to base line. A basic curve fitting technique, Method 3, shown in Figure 2.9 similar to Method 1 was employed but in this case the end points were zero crossing points and the peaks. The MATLAB functions ‘fit’ and ‘fittype’ were used to find the best fit line. Also, the function ‘interpl’ in MATLAB was used in some scenarios if the coordinates of peak were not available in the ‘wave’ array. The elevation or the perpendicular distance between the baseline and the peaks are calculated by finding the voltage difference between the baseline and the corresponding peak points. This is shown as PD1, PD2 and PD3 in the Figure 2.10. This MATLAB code has been added in the Appendix part of the thesis.

Chapter 3

Results and Discussions

3.1 Specific Aim 1

Single Unit Spikes (SUS) were recorded across all the modalities as early as one week post-injury from 1 animal and recorded until 42days post surgery. The entire study involved non-repetitive (present in one of the modalities) and repetitive (present in more than one modality) single unit spikes corresponding to Wake (control), Heat stimulus and Mechanical stimulus. Various parameters, such as the average spike amplitude, average firing rate, depolarization time of the average spike; extracted from the raw neural data have been considered for this evaluation.

Throughout this study, all graphs have been plotted considering each point as individual spike unit. The number of animals is not uniform and ranges from 1 to maximum 6, at a given time point. The number of single unit spikes and the number of animals considered at each time point for the study in Section 3.1, are tabulated as shown in Table 0.1.

Table 0.1: Number of animals considered for measurements at each time point

Days Post Implantation	Number of Single Unit Spikes			Number of animals
	Wake (Control)	Thermal	Mechanical	
7 Days	3	6	2	**1**
14 Days	16	13	15	**6**
21 Days	18	25	19	**7**
28 Days	5	7	6	**3**
35 Days	3	2	0	**2**
42 Days	4	2	2	**2**

3.1.1 Specific Aim 1: Firing Rate

The firing rate of single unit spikes that were recorded every week beginning from 7days post implantation is represented in Figure 0.1. As observed, the sample size of single unit spikes on day 7 and post day 35 is low (i.e. less than 3). The maximum single unit spikes were recorded at Day 14 till Day 28 across all the sensory sub-modalities. One-Way Anova followed by non parametric Kruskal-Wallis post-hoc test was used to statistically analyze the data. We also noted that the mean firing rate of all the units were comparable across all the sub-modalities corresponding to each time point; however, comparing each group of SUS with the other, tested statistically insignificant between all the groups as shown in Figure 0.1.

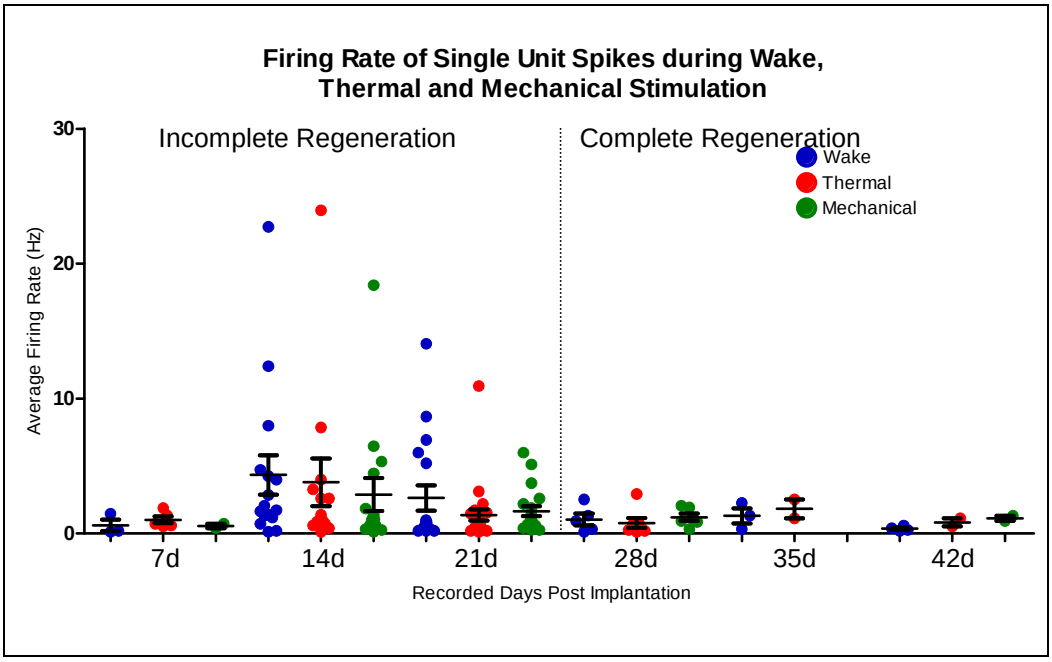

Figure 0.1: Shows firing rates of Single Unit Spikes recorded at weekly time points of day 7 to day 42 post-implantation during Wake, Thermal and Mechanical Stimulation. (One – way ANOVA, Dunn's post hoc test, $P<0.05$, Mean±SEM)(Incomplete Regeneration: Not reached end organ; Complete: reached end organ)

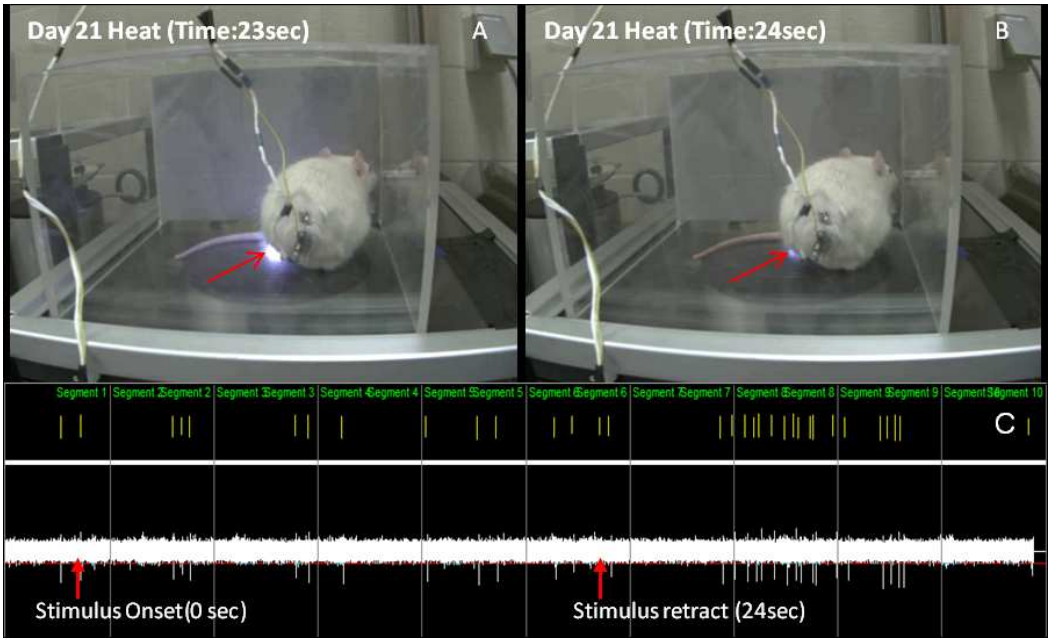

Figure 0.2: Shows changes in firing pattern; A) Stimulation via Infrared Beam, B) Stimulus retract, C) Neural recording during stimulation

Based on above observations, each recorded SUS was visually examined (when the injured limb was subjected to thermal stimulation), revealing an instantaneous change in the firing pattern during the course of stimulation. This firing pattern change was demonstrated at day 21 post implantation in 10 SUS in 7 animals, after the stimulus was withdrawn. In Figure 0.2A-C, it is shown that while the stimulus was being applied, the firing pattern was more dispersed and once the stimulus has withdrawn; there was burst spike activity.

Neural activity recorded at 7, 35 and 42 days was not included in this comparison as the sample size was small to run a statistical test. However, data for 14days revealed a more repetitive tonic firing pattern during and post stimulation as illustrated in Figure 0.3.

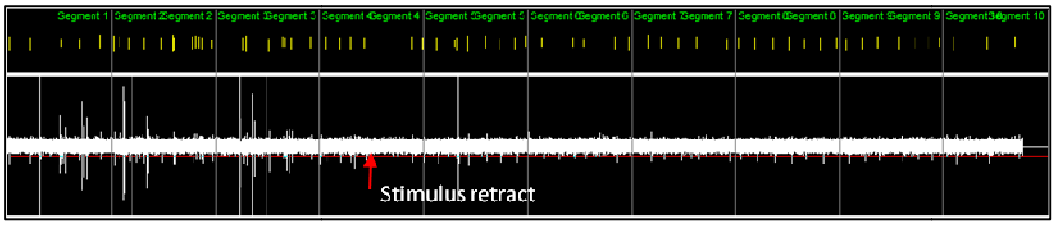

Figure 0.3: Screenshot showing repetitive firing pattern during and after stimulation in an animal recorded at 14days post implantation. Red arrow signifies the instant at which the stimulus was withdrawn.

The average firing frequency recorded while subjecting the injured paw plantar surface to heat stimulus delivered by infra-red beam and recorded after the stimulus was retracted, was quantitatively compared for time points 14, 21 and 28 days post implantation. Figure 0.4 demonstrates that the firing rate mean increased from 0.5 - 2.5spikes/sec and 0 - 2spikes/sec for 21days and 28 days respectively after stimulation as compared to while stimulating, but on day 14 the firing pattern was essentially unaltered throughout the stimulation time and also after the stimulus was removed, for all 13 Single unit spikes recorded in 5 animals exemplified in Figure 0.4.

The data was tested for statistical significance using one-way ANOVA followed by a non-parametric Kruskal-Wallis post-hoc test (α=95%), showing significant incremental difference in rate of action potential generation. Unpaired Two-tailed T-test was used for analysis that confirmed no significant difference between the two firing rates (α=95%). 2 units from two different animals had a repetitive ongoing activity with a firing frequency represented by the 2 highest samples (Figure 0.4); also there were three units that had an increased firing frequency after the withdrawal of the stimulus and one unit that maintained a repetitive firing rate during the process of stimulation and firing rate dropped to 1 spike/sec immediately after removing it.

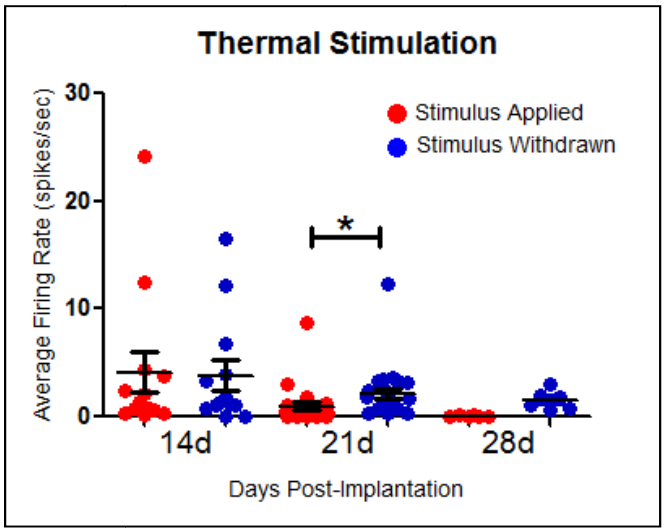

Figure 0.4: Distribution of average firing rate showing Thermoceptive sensory SUS (Red) and Proprioceptive motor SUS (Blue)

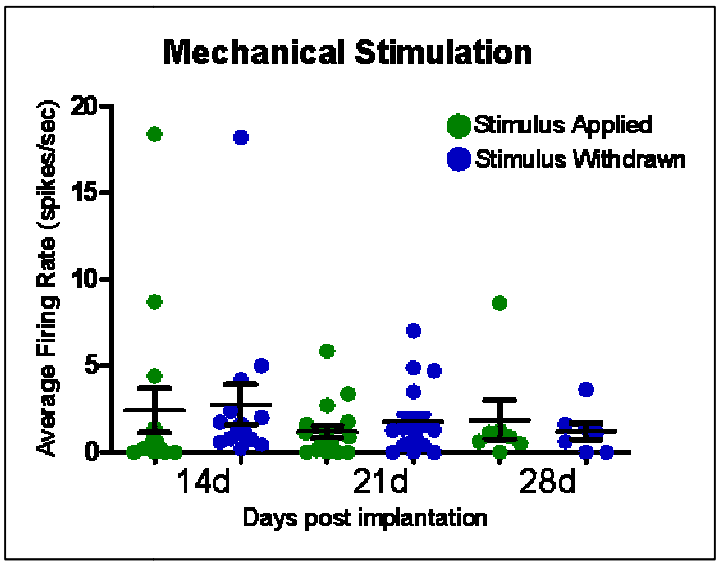

Figure 0.5: Distribution of average firing rate showing Mechanoceptive sensory SUS (Green) and Proprioceptive motor SUS (Blue). (P<0.05, Mean±SEM)

Similarly, single unit spikes recorded while stimulating with the Von-Frey hair and post paw withdrawal response were evaluated in terms of firing rate as demonstrated in Figure 0.5. The graph represents all the unit spikes recorded across day 14, 21 and 28

days post stimulation and it is observed that the mean of each group is similar. Day 7 and 42 was excluded from the statistical analysis because of low sample size (size=2). At day 35, none of the experimental animals recorded single unit spikes during mechanical stimulation. Initially unpaired Two-tailed T-test was used for analyzing the firing frequency of each time point individually, that showed no significant difference between the two firing rates (α=95%). Repeated statistics between all the groups using one-way ANOVA followed by a non-parametric Kruskal-Wallis post-hoc procedure (α=95%) also confirmed no significant difference in firing rates before response and after response to the Von-Frey hair mechanical stimulation.

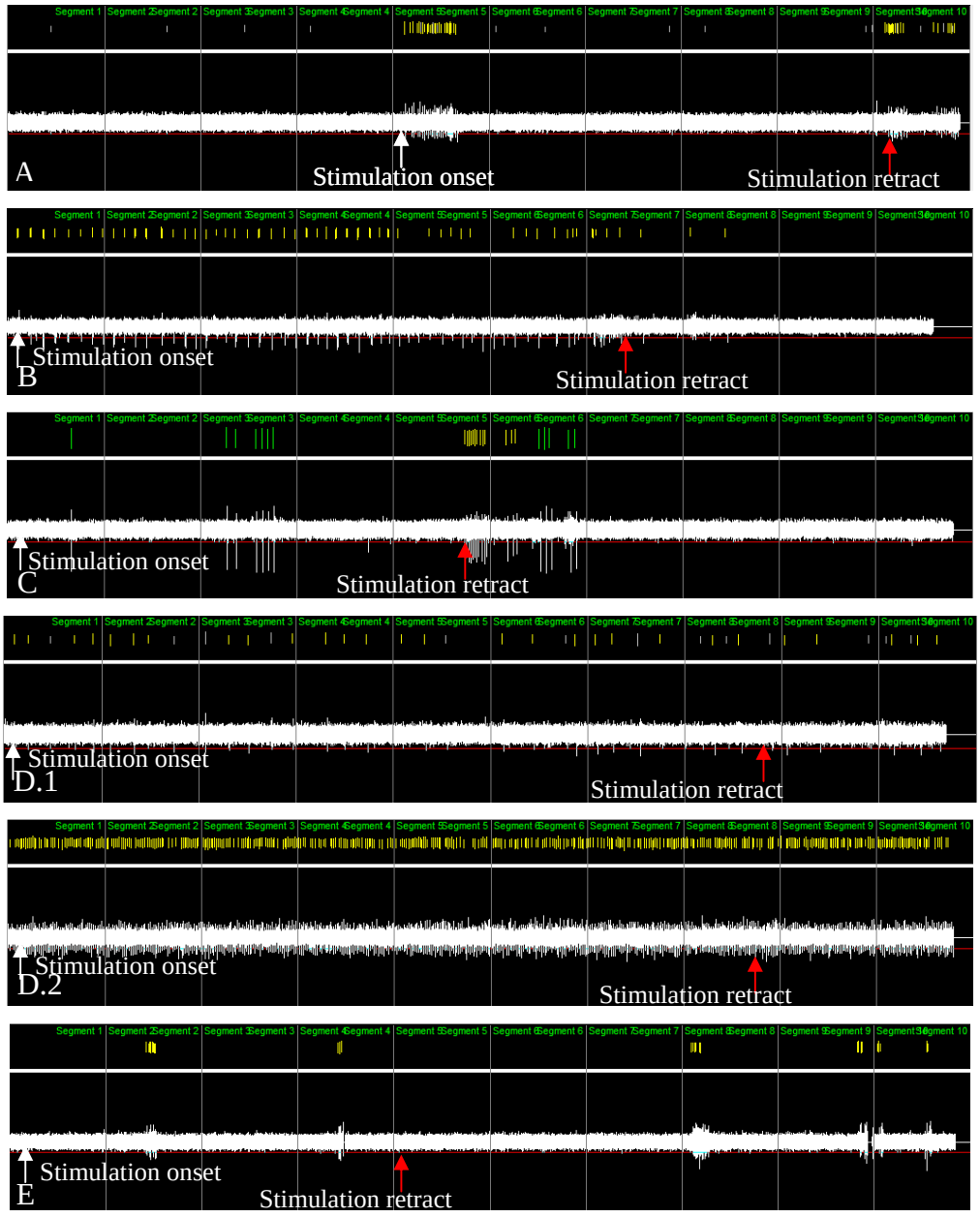

Figure 0.6: Various firing patterns observed in single unit spikes recorded for mechanical stimulation. A) Burst firing pattern marking onset of stimulation and instant of stimulus withdrawal in an animal recorded at 14days post implantation. White Arrow: Onset of stimulation; Red arrow: Stimulus was withdrawn. B) Repetitive firing during stimulation only. C) Spike burst at withdrawal (yellow: possible motor unit). D) Repetitive firing during entire recording with no correlation to the stimulation. E) Random Spike activity with no correlation to the stimulation

Although statistical analysis showed no significant difference in the firing rate when all the units were examined together but several firing patterns were observed when each unit was inspected independently. This visual inspection revealed 5 different patterns in a total of 39 units across 14, 21 and 28 days post implantation as illustrated in Figure 0.6(A-E). Three units in the same animal showed bursts at the onset of stimulation and paw withdrawal, recorded at 14 day; however, this pattern was not seen in any other animal at other time points (Figure 0.6A). 6 animals across 14, 21, 28 days showed rhythmic spikes till the stimulus withdrawal and then continued with low activity or stopped firing (Figure 0.6B). Also, five units were identified in correlation with the paw withdrawal motor response of the animal as neural spikes were observed while the animal moved its limb and no activity was observed before the response or after the animal had stabilized post response (Figure 0.6C). Figure 0.6D shows non-correlated neural activity observed in animals having repetitive firing. 8 units showed random spike activity throughout the recording time (including during and post stimulation). The irregularity in the pattern varied from segments of bursts alternated with phases of no activity (Figure 0.6E) to spikes with wide ranging inter-spike intervals.

3.1.2 Specific Aim 1: Amplitude and Wave Shape

This section aims to address the average amplitude and parameters defining spike shape of action potentials, recorded in response to thermal and mechanical stimulation of the injured limb. The approach of amplitude/wave-shape is established on the presumption that different types of neurons generate different wave forms of spikes (Abeles and Goldstein, 1977). All the recorded SUS were processed as discussed earlier in the section 2.5.2. The amplitude of average waveform with the error bars representing standard error mean, was considered to compare between wake (control), thermal stimulation and mechanical stimulation. Graph in Figure 0.7 shows that the distribution of

average amplitude (in μV) of unit spikes was comparable between modalities across all time points. P values <0.05 were considered to be statistically significant. One-way ANOVA Kruskal-Wallis statistics followed by Dunn's post-hoc test for multiple comparison, showed no significant difference between the groups within a time-point.

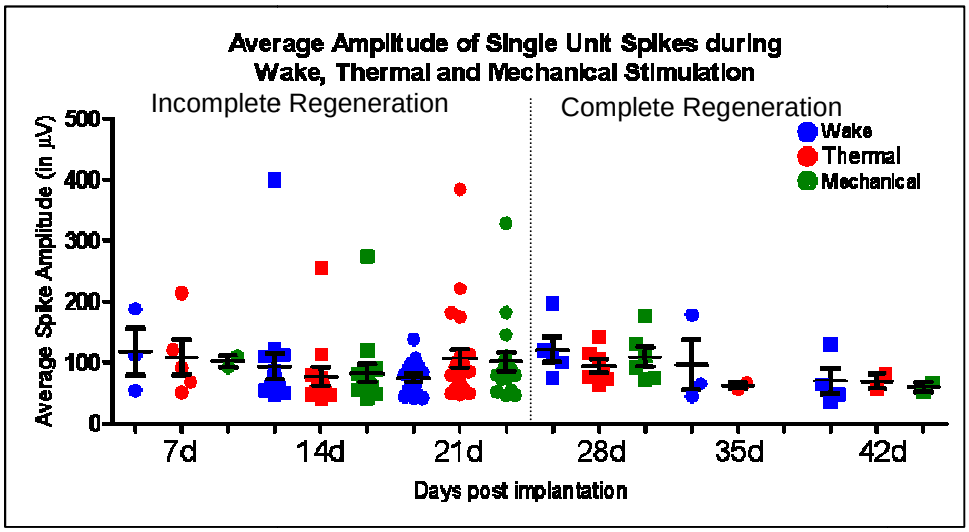

Figure 0.7: Average Amplitude of all Single Unit Spikes generated in response to wake, Thermal and Mechanical Stimulation. No significant difference between groups across all time points (P<0.05).

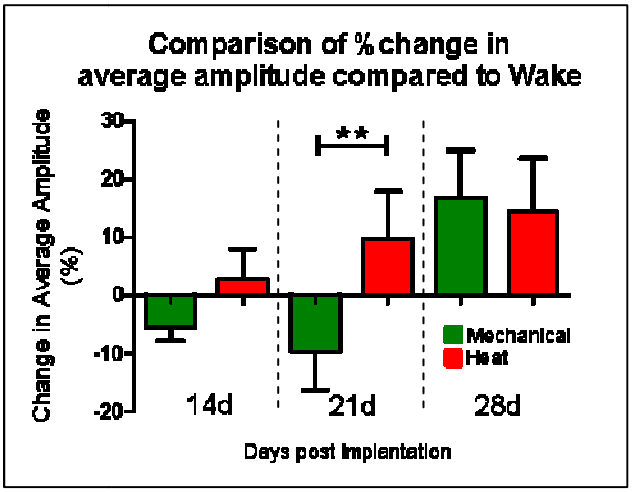

Figure 0.8: Change in Average amplitude of repetitive units during Thermal and Mechanical stimulation with reference to wake (No stimulus). (Mean±SEM, P<0.05)

However, only repeated SUS (present in wake and mechanical and/or thermal) were considered for comparison and percentage change in average amplitude in heat (or mechanical) with reference to wake (non-stimulus/control) within the same time-point showed a significant difference for time point: 21 days and no difference at other time points (Figure 0.8). One-way ANOVA (non-parametric) followed by Dunn's comparison post-hoc test was applied to test Statistical significance ($P<0.05$).

The action potential was divided into three segments with reference to spike shape: *1*) a brief, positive peak; *2*) a much larger negative peak; and *3*) a positive period of longer duration and slowly decaying amplitude for a comprehensive study as discussed in section 2.5.2.

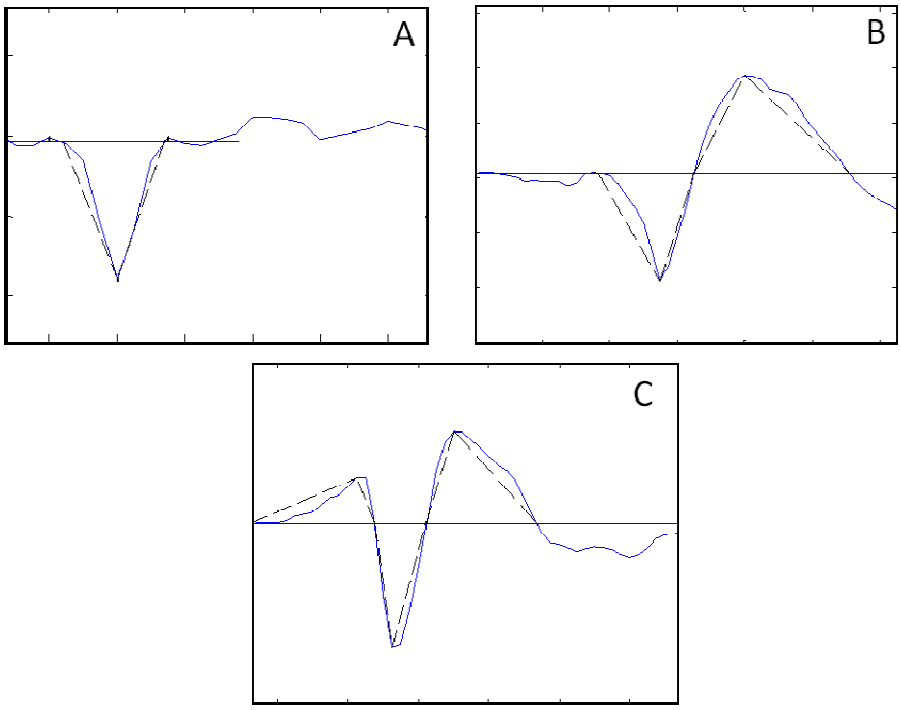

Figure 0.9: Spike shapes defined by absence/presence of Initial Peak. A) Monophasic, B) Biphasic waveform, C) Triphasic waveform. (Blue horizontal line marks the signal baseline, black dashed line is linear representation of the action potential wave shape)

Presence or absence of the peaks was utilized as a parameter to define spike shapes as monophasic, biphasic or triphasic. By considering a threshold value <10μV, 8 spikes were monophasic (only negative peak), 59 units were biphasic (initial peak absent) and 75 units were triphasic (all peaks present). Examples of each type of unit are illustrated in the Figure 0.9(A-C). As observed in the data set, all the monophasic SUS had average total amplitude of <50μV, whereas biphasic and triphasic units had a wider range of average total amplitude >50μV to as high as 400μV. Monophasic units were predominantly identified during recording in freely moving animal with no specific external stimulus though biphasic and triphasic was seen in all the modalities at all time points. Another significant observation was that spike duration was significantly correlated with undershoot amplitude (third peak)

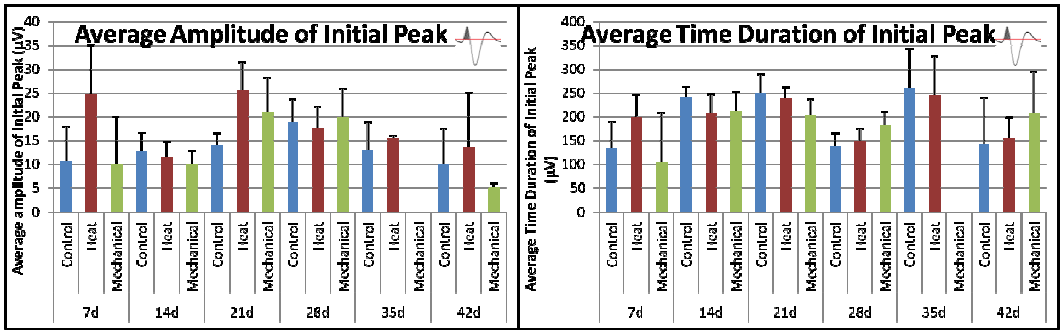

Figure 0.10: Histogram of average amplitude of initial peak of all units recorded across various times points during sensory submodalities (mean±SEM)

Each segment is then analyzed for its amplitude and time duration, consequently resulting six measurements to represent a single unit. The first phase, characterized by amplitude and time duration of the initial peak of spike, is caused due to the positive capacitive current (Gold et al 2006). Figure 0.10 shows that the amplitude of single unit spikes ranged between 0 to 160μV. However, statistically One-way ANOVA with Dunn's

comparison post-hoc test and two-tailed T-Test showed no significant difference between the modalities at any time-point ($P<0.05$). Similar assessment of average time duration of the initial peak of evoked potentials ranging between 0 to 500μs approximately, during the modalities showed no statistically significant difference.

Average amplitude and time duration of the negative peak (2nd peak) and last positive peak (3rd peak) were analysed with identical statistical tests (One-way ANOVA with Dunn's comparison procedure and T-Test) which also showed no significant difference in any of the parameters (shown in Figure 0.11, Figure 0.12 respectively).

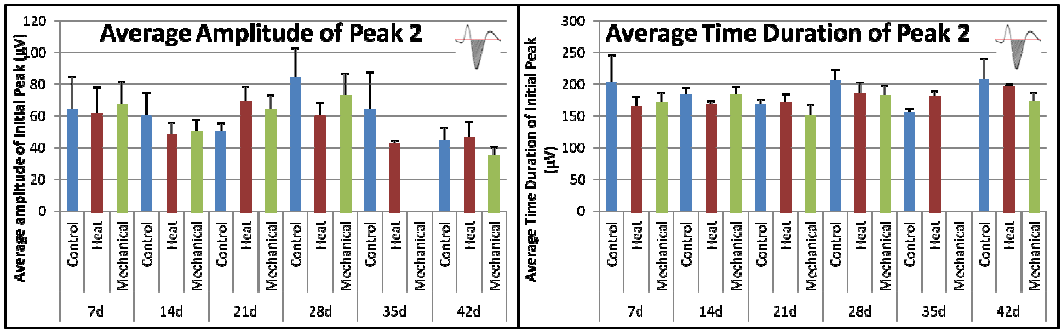

Figure 0.11: Histogram of average amplitude of initial peak of all units recorded across various times points during sensory submodalities.

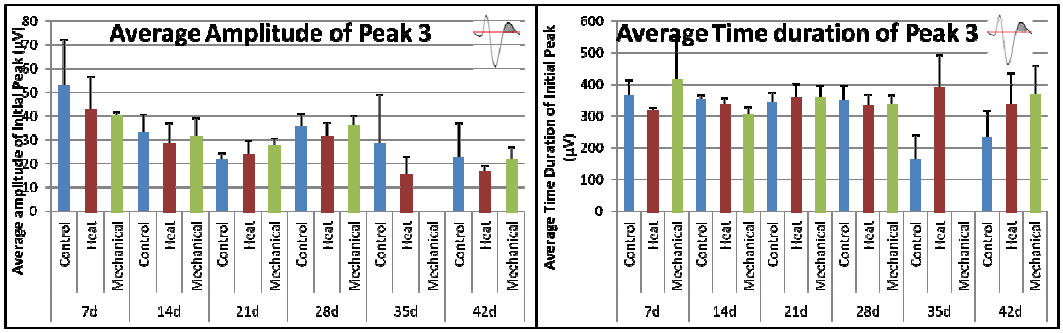

Figure 0.12: Histogram of average amplitude of initial peak of all units recorded across various times points during sensory submodalities

3.1.3 Discussion

Neurons are known to represent and transmit a dynamic range of information by firing sequences of spikes in various temporal patterns; however, typically many neurons

respond to a given stimulus, and stimulus features are therefore encoded by the activities of large neural populations (Hodgkin et al. 1952, Dayan et al. 2000). The firing rates of sensory nerves encode the stimulus magnitude and also the time course of stimulation. The temporal properties of a stimulus are encoded as changes in the frequency of sensory neuron activity. From the results described above it can be concluded that neurons typically transmit information in various patterns of firing namely: random, repetitive (tonic) and bursts (phasic). Also, neurons' signal properties of stimuli not only when they fire but also when they stop firing as we have seen in Figure 0.6.

This study aims to record evoked potential from a mixed regenerating nerve across sensory sub-modalities in a freely moving animal and identify SUS in terms of their firing rate. The results revealed single unit spikes that were evoked during single modality as well as multi-modalities including spontaneous activity with no signature firing pattern specific to each sensory sub-modality. To address the underlying reason for the above observation each SUS was independently examined.

During thermal stimulation, statistical analysis showed that firing rate significantly increased just after the stimulus was withdrawn and the pattern of firing was primarily phasic in majority of the unit spikes recorded for 21 and 28 days post implantation. Previous researches have stated that rat foot withdrawal responses evoked by a high rate of skin heating are mediated primarily by the activation of myelinated Aδ nociceptive afferents, while responses evoked by a low rate of skin heating (<0.9º/sec) are mediated primarily by activation of unmyelinated C-fiber nociceptors (Yeomans et al 1996). A graded increase in the skin temperature from the normal value (around 30℃ with an ambient temperature of 20℃) to within the noxious range, prompts successive activation of thermoreceptors and then C- and A- polymodal nociceptors (Le Bars D. et al 2001) 0followed by polymodal nociceptors, high-threshold mechanoreceptors, and cold

receptors, thus contributing to the random firing pattern in extracellular recordings and making differentiation between the units more challenging.

Similarly, Mechanical stimulation showed a wider variety of firing patterns across the time points and as Aδ-fibers is predominantly sensitive to mechanical stimulation i.e. pricking pain (Adrian 1928), hence we can conclude that units that showed stable firing during the course of stimulation were Aδ-fibers. Thus single unit spikes recorded during graded thermal stimulation that showed increased firing may have resulted due to activation of C-fibers followed by Aδ-fibers denoting nociceptive pain.

Some units showed a repetitive tonic activity through the course of recording which might be explained as neuropathic pain caused due to ectopically generated impulses by the sympathetic nervous system. Following a peripheral nerve injury, sympathetic postganglionic fibers are said to sprout into the DRG which contains somata with lesioned axons (Ramer and Bisby, 1997). It is also noted that lesioned primary afferent neurons endure biochemical, morphological, and physiological transformations expressed in up- or down-regulation of voltage-gated ionic channels, transduction channels for physiological stimuli, membrane receptors for various chemical (in particular inflammatory) mediators, and the intracellular pathways coupled to them (McMahon et al. 2006, Djouhri et al. 2012). In general the injured primary afferent neurons switch to a state of regeneration, sprouting at the lesion site as well as proximal to the lesion site in the nerve primarily resulting in ongoing pain, evoked ectopic excitability, mechanical, or thermal allodynia in both A-fibers and unmyelinated C-fibers (Devor et al. 1999, Devor 2006, Baron 2008, Gorodetskaya et al. 2003, Grossmann et al. 2008). Furthermore, after sciatic nerve transection low threshold mechanosensitive fibers begin to express substance P (Noguchi et al. 1995) causing sensitization in DRG neurons (Yaksh et al 1999). Secondly ectopic activity may arise in afferent Aδ-fibers that were originally

connected to high threshold mechanoceptors. The burst discharge in several neurons may evoke central sensitization thus causing abnormal pain (Liu et al. 2000). Since we recorded from a mixed nerve we do not know the proportion of sensory to motor axons among those spontaneously active. However, previous studies suggest that most, but not all, of the spontaneous activity is carried in sensory fibers (Govrin-Lippmann et al. 1978).

Also some of the spikes recorded, were strongly correlated to the movement of the animal (as seen in video clips) in response to the stimulation, thus could be explained as possible motor unit activity (in Figure 0.6c).

Mechanical and Thermal stimuli were used to excite non spontaneous units from the mixed nerve and several spikes were averaged for further analysis of the spike shape. Six measurements of spike shape were made as discussed earlier dividing the complete spike shape into 3 segments.

Considering the mechanism of the entire action potential, this process of evaluation was based on differences in each neuron's extracellular waveform that are initiated from cell-specific biophysical properties. There are evident differences in axonal spike shape between the different functional classes of fibers and, in particular, A-fibers tend to have larger amplitude and shorter duration in contrast to C fibers, specifically nociceptive C-afferents tend to have axonal action potentials of longer duration than non-nociceptive afferents; however, sympathetic postganglionic axons in rats, have spikes of longer duration than afferent axons (Gee et al 1999). These fibers were first identified in a sural nerve using conduction velocities and then correlated to spike shaped using electrical stimulation. Research by Gee and Lynn state that, the ion channels distribution can be responsible for the differences in spike duration seen in spikes generated by different functional classes of unmyelinated axon (Gee et al 1999).

As discussed in the results, graded increase in temperature triggers successive activation of multiple fiber types namely classes of thermoceptors and mechanoceptors. And mechanical stimulation using a Von-Frey filament has been revered as a standard in studies for behavioural test (Handwerker and Brune, 1987), but it has the disadvantage of activating low-threshold mechanoreceptors as well as nociceptors simultaneously thus making discrimination between units from individual fibers in an extracellular recording difficult. When neural activity is synchronous between neighboring cells, there is considerable overlap of the spike waveforms and sorting individual clusters becomes very difficult (Hill et al 2011). The current approach considers the voltage only at a particular time point, whereas extracellular waveforms have characteristic shapes that extend over many data samples.

Also, somatosensory anatomy reveals that each sensory receptor has a specific location in space that transmits information. This spatial receptive field is sensitive to external stimulus thus affecting the receptor cell or sensory neuron to respond (Wedell and Miller, 1962). The receptive fields of individual sensory receptors may overlap partially/completely with one another such that any given stimulus to the human skin can potentially stimulate a large number of nerve terminals, for example a mechanoreceptive stimulus can be detected by several nerve endings sharing the same receptive field. Therefore, correlating evoked action potential wave shapes to specific fibers in a mixed nerve could not be clearly defined.

Lastly, neural interface is said to involve considerable amount of variability due to micromotion of the interfacing electrodes that are embedded in the nerve tissue. Micromotion at the interface result in continuous injury related biological mechanisms like inflammation and scar formation, which may account to the change in neural activity

parameters. Therefore, the next section involves the study done to test the stability of the average wave shape parameters.

3.2 Specific Aim 2: Immediate Effects of Limb Stretching on the wave shape

The goal was to study the changes in the spike shape of the REMI recorded compound nerve action potential (CNAP) after nerve stretch and compare them to the spike shape seen before nerve stretch. The typical spike shape was divided into three segments as described previously in this study for a detailed analysis CNAP amplitudes and duration.

Table 0.2: Number of units at each time point against change in the total amplitude in post-stretch compared to pre-stretch

`	*No Visual Change in shape with <10% change in total amplitude*	*No Visual Change in shape with >10% Increase in amplitude*	*No Visual Change in shape with >10% Decrease in amplitude*	*Total number of units*
7 Days	**10**	**2**	**2**	**14**
14 Days	**4**	**5**	**1**	**10**
21 Days	**2**	**1**	**0**	**3**
28 Days	**0**	**0**	**3**	**3**
Total Units Per group	**16**	**8**	**6**	**30**

The total number of units that were recorded during this experiment was 71 from nine animals across 7, 14, 21 and 28 days post implantation including 70% and 100% stretching. Among these, only thirty specific units were present during pre-stretch as well as post-stretch recordings and 32 units were lost after stretching and nine units were activated post stretching. Thus, this study is focused on the evaluation of the spike shape of the 30 units that continued activity after stretching. All the SUS had comparable shape characteristics, before and after the limb was subjected to cyclic stretching.

Table 0.2 shows the distribution of all the units based on increase, decrease or no change in amplitude. By visual inspection the SUS was marked with 'No change' if four out of the six parameters have below Δ20% with reference to pre-stretch recordings. Figure 0.13 demonstrates that the mean percentage change in both the groups was comparable and >5%. Statistical analysis using a paired two tailed T-test with 95% confidence intervals, showed no significant difference (P=0.9112).

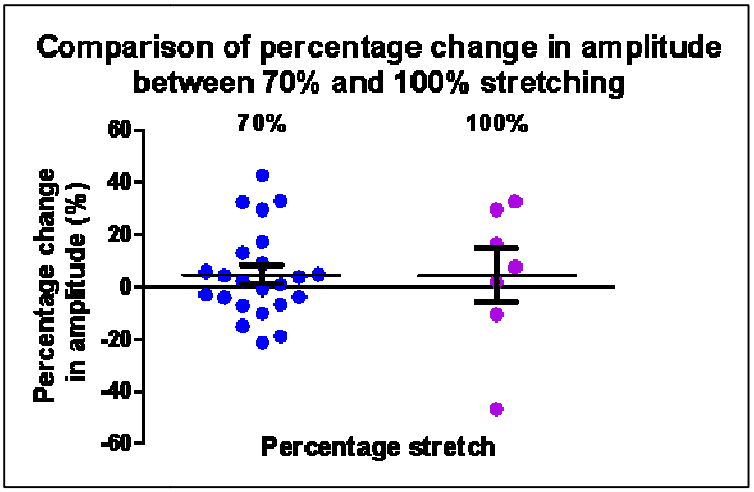

Figure 0.13: Percentage change in amplitude of SUS post stretch (70% and 100%) compared to pre-stretch

A typical representation of a SUS showing 'No Change', (all six parameters are within 20%) recorded before and after a stretching cycle is shown in Figure 0.14.

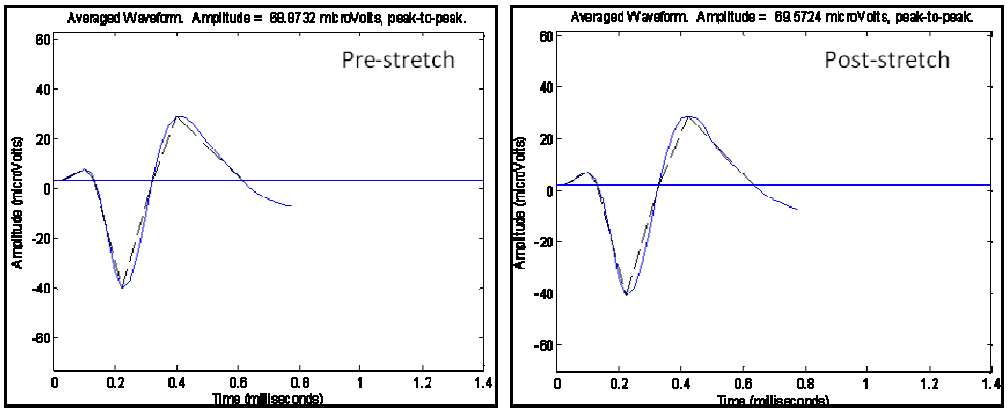

Figure 0.14: Typical SUS recorded at 21 days showing equal amplitude and similar shape

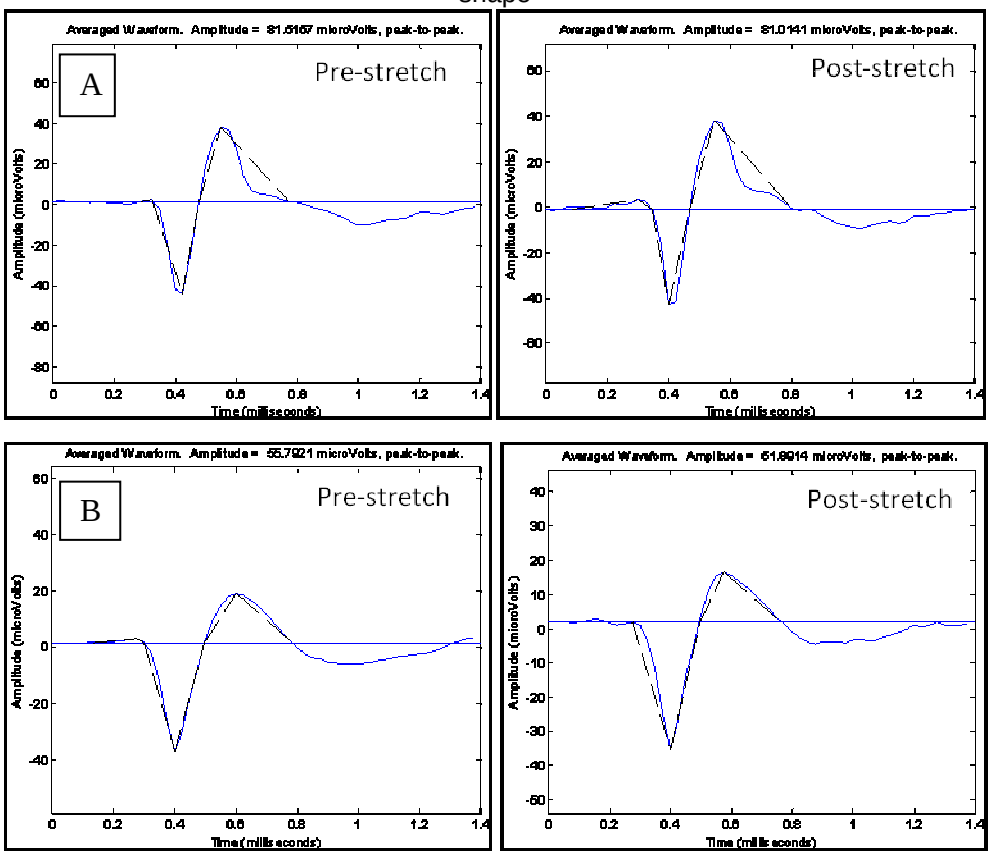

Figure 0.15: Units having >50% change in the amplitude and time duration of initial peak. A) Increase of 62% in time duration; B) Decrease of 54% in time duration.

Figure 0.15 shows 2 unit spikes waveforms that were considered as 'No Change' because of same total amplitude; however, time duration and amplitude of the initial peak had a difference of 50%, which can be explained because of the change in reference position due to signal baseline variability.

Evaluating the amplitude and time duration of each of the three segments, it was observed that there was no significant difference between the single unit spikes recorded before and after stretching the limb in a cyclic pattern. As shown in Figure 0.16, Figure 0.17 and Figure 0.18, the mean at each time point (considering 70% and 100% together) were comparable between the two groups with marginal difference. One way ANOVA followed by Dunn's post-hoc comparison test showed no statistical significance.

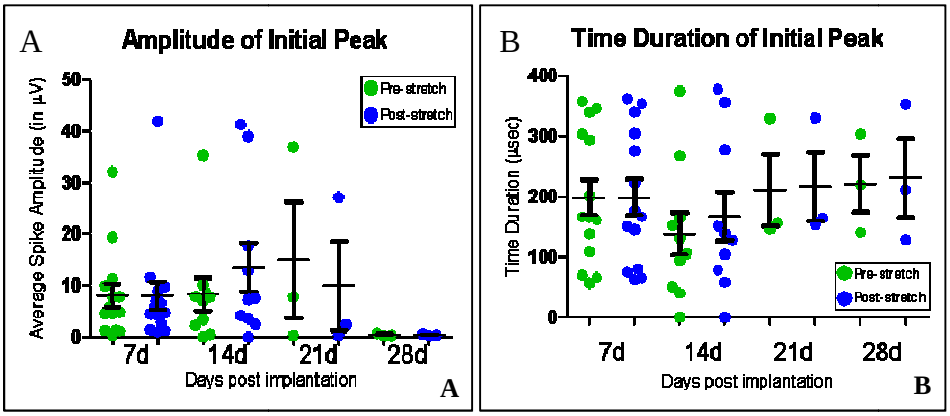

Figure 0.16: Graph showing comparison of initial peak (Positive capacitance current) of SUS post-stretch with pre-stretch A) Amplitude B) Time duration

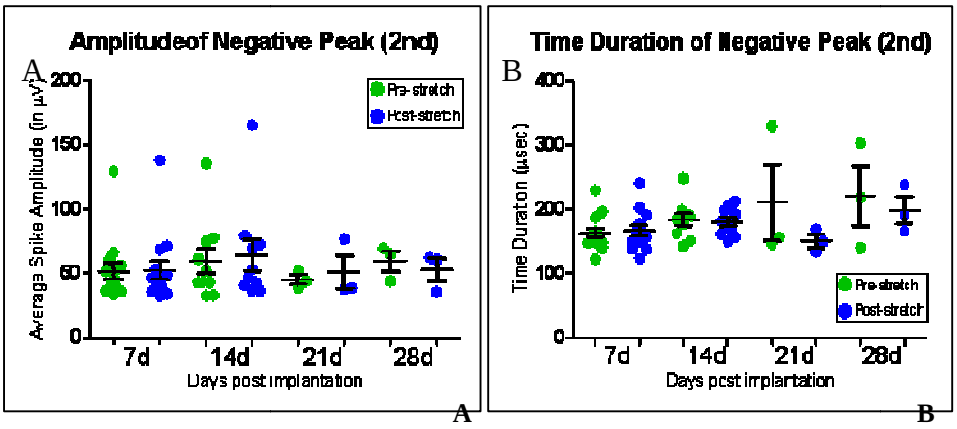

Figure 0.17: Graph showing comparison of Negative peak (Current due to Na+ ion influx) of SUS post-stretch with pre-stretch A) Amplitude B) Time duration

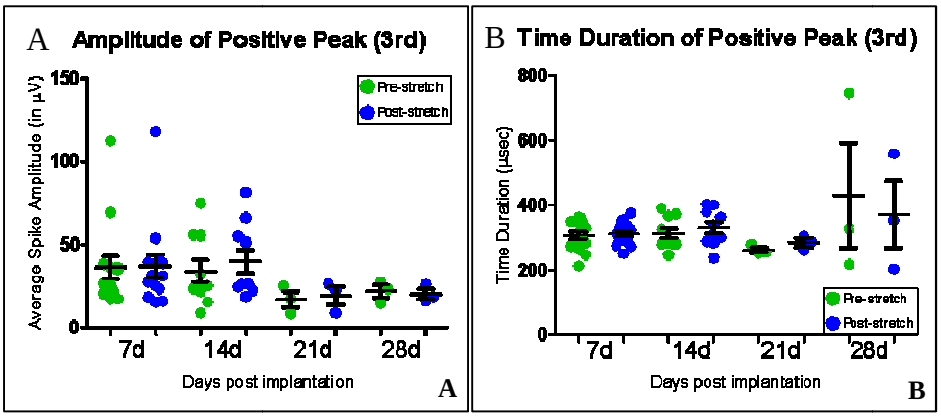

Figure 0.18: Graph showing comparison of Positive peak (Current due to K+ ion flowing out of cell) of SUS post-stretch with pre-stretch A) Amplitude B) Time duration

Additionally, it was observed that the firing rate did not change significantly after stretching, although 8 units showed a decrease in firing rate of 1spike/sec; 1 reduced by 5 spikes/sec and 1 unit increased by 6 spikes/sec. Statistical analysis using a Student paired 2-tailed T-Test comparing (70%and 100%) pre and post stretch together revealed no significant difference; however, within 100% stretch group there was significant decrease (p=0.0165) as illustrated in Figure 0.19.

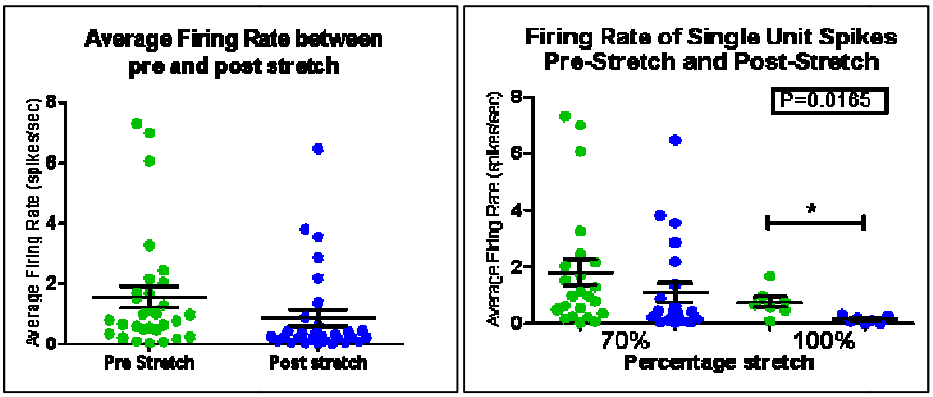

Figure 0.19: Graph showing firing rate of post -stretch compared to pre-stretch. A) All stretch considered together B) 70% and 100%

3.2.1 Discussion

Previously (Watson 2012), it has been examined that natural limb motion, as simulated in this experiment, did not cause any detrimental effect on the nerve with the electrode interface with respect to scar tissue formation or decrease in axonal regeneration; instead enhanced regeneration of the nerve which confirms that exercise induces increase in BDNF thus facilitating nerve regeneration (Wilhelm et al. 2012). The aim of this study was to quantify any change in spike shape parameters as an immediate effect of cyclic stretching.

Research review on the stretching mechanism reveals that the sensory stimulation that excites stretch-activated channels (Del Valle et al 2012) are regulated primarily by low-threshold Aα and Aβ nerve fibers present in the neuroma (Proske et al. 1995) and originating from mechanosensory neurons in the dorsal root ganglion. These stretch-activated ion channels respond to mechanical deformation of a neuronal plasma membrane by opening their pores, resulting in depolarization in the afferent neuron and production of action potential with adequate depolarization (Purves et al 2004).

Hodgkin in 1954 and Goldman in 1963 proposed that stretching initially smoothen folds in the membrane such that there is no alteration in the true surface area

of the fiber and thus maintaining the conduction velocity constant. Studies based on stretch due to limb lengthening, (Jou et al 2000) suggest that a 50% change in amplitude of a somatosensory evoked potential is associated with a clinical deficit due to stretching of the peripheral nerve. Therefore, as our amplitude change was within 10%, it can be concluded that the normal limb motion due to cyclic stretching did not affect the shape of the action potential when recorded immediately post stretching. Fowler stated that the sciatic nerve of a rat could tolerate 50 gm of stretch for two minutes before causing permanent injury. Also the nerve within the nerve guide tube is known to regenerate-myelinate and reinnervate to original distal organs beyond 30 days (Wall et al. 1979). Therefore, a totally regenerated nerve may exhibit different mechanical properties and spike shape parameters prevailing due to stretch. The peak to peak amplitude was more variable during the nerve stretch experiments but both conduction velocity and amplitude are abnormal when there was a high level of stretch (Stecker et al 2011). Similarly, this can account for the unaltered firing rate observed post 70% stretching (Figure 0.19). However, the firing rate reduction for 100% stretching may be explained by possible mechanical damage due to strain on the nerve, altering conduction properties of fibers (Stecker et al 2011).

Chapter 4

Conclusion and Future Scope

Several studies in cortical interface have achieved to provide motor control for neuralprosthesis, like Tarkka and Hallett attained mapping of the movement-related cortical potentials close to the commencement of EMG activity correlating to finger and toe movements (Tarkka et al 1991). Another research focuses on electrical stimuli in primary somatosensory cortex for restoring perception of intensity of a mechanical probe indented into the hand (Hsiao et al 2011). Peripheral neural interface have proved the probability of sensory feedback and rationale of attaining motor commands for robotic prosthetic limb control. This study was aimed at interfacing sensory modalities like thermal pain, mechanoception and stretch induced activity in a regenerating transected mixed nerve using the REMI in a freely moving animal.

We analyzed the neural activity on the basis of its firing frequency that revealed no significant difference between sub-modalities but different discharge patterns were identified. These patterns included random, repetitive (probable spontaneous activity), sensory evoked and motor units. Similarly, evaluation of shapes of single unit spikes associated to the modalities demonstrated no significant change across sensory sub-modalities even though units were recognized as monophasic (few), biphasic and triphasic waveforms. Therefore, defining signatures in firing rate and amplitude with spike shape corresponding to the stimulus was challenging because of probable continuous ongoing activity due to sympathetic pain and successive activation of different types of fiber-receptor due to the application of graded stimulus.

Secondly, specific aim 2 was based on the effect of stretching on the conductivity of the nerve fibers. We did not observe any statistically significant change in the firing rate or the spike shape parameters post stretching as compared to activity prior to

stretching. This observation may have resulted due to not sufficient stress application on the nerve. Also, we did not evaluate experimentally, the effect on the activity while the limb was stretched due to possible motion and muscle activity infiltration.

However, in addition to the wave shape parameters that were discussed earlier in Section 2.5.2, a possible parameter that could be considered, is the Area under the curve for each phase of the average waveform. The area can be calculated with an alternate approach of Gaussian Approximation curve fitting as an alternative to the linear approximation method used in the current study. In order to facilitate this approach for future work, this method has been implemented for a minimal set of data. A comparison of area under the curve has been shown in the Table 4.1, for this set of data. Figure 4.1 represents the first phase (rising phase) of the action potential wave. In this figure, the blue specks represent the Average Wave Data and the red line represents the respective Gaussian approximation. Similar representations for the phase 2 and phase 3 have been shown in the Figure 4.2 and Figure 4.3 . The area under the curve is calculated the integral of the Gaussian function with the limits being the start and end time of the phase. The integration and the Gaussian fit have been implemented in MATLAB. The code is added in the Appendix A.

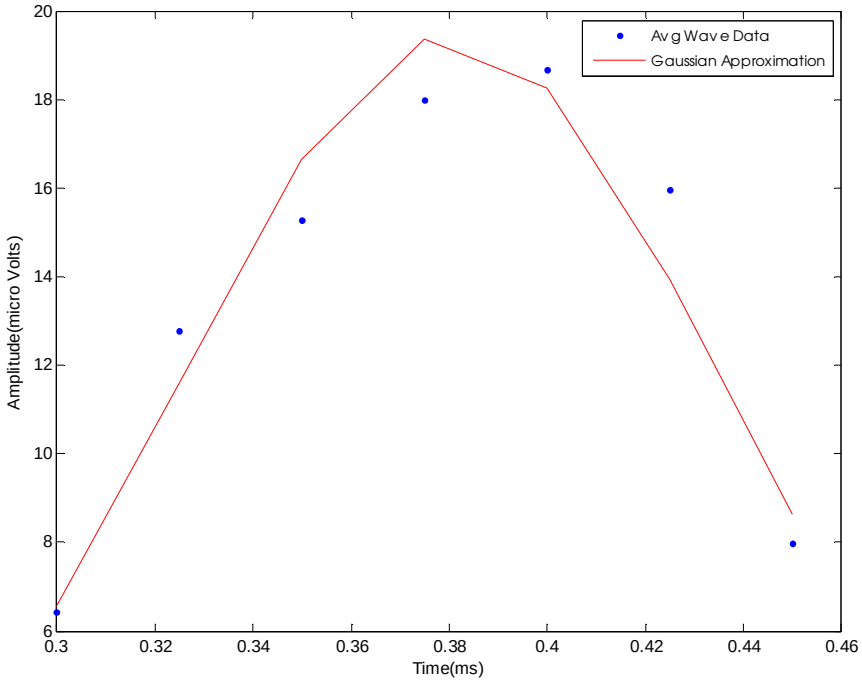

Figure 4.1: Representation of Phase 1 of Action Potential with a Gaussian Approximation curve fitting method.

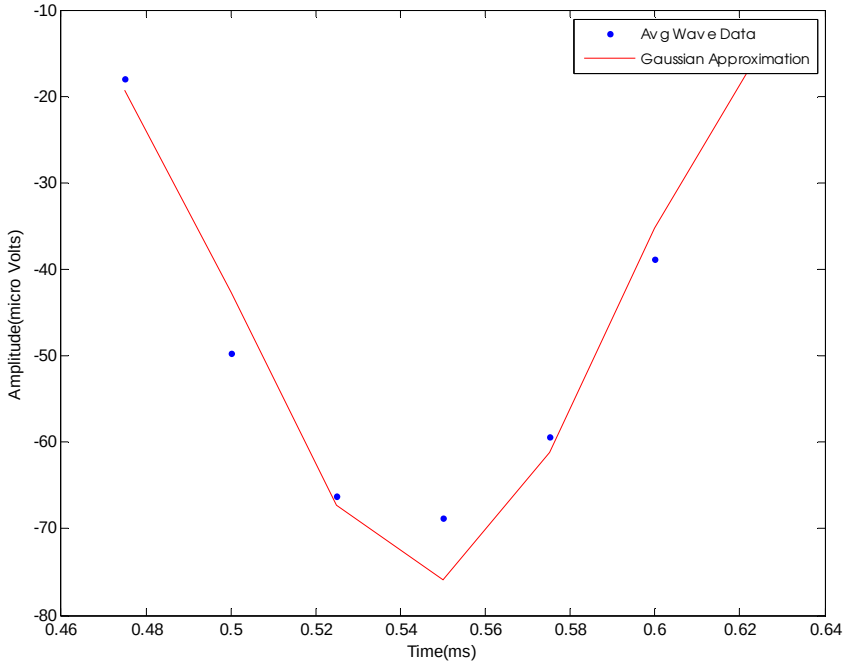

Figure 4.2: Representation of Phase 2 of Action Potential with a Gaussian Approximation curve fitting method

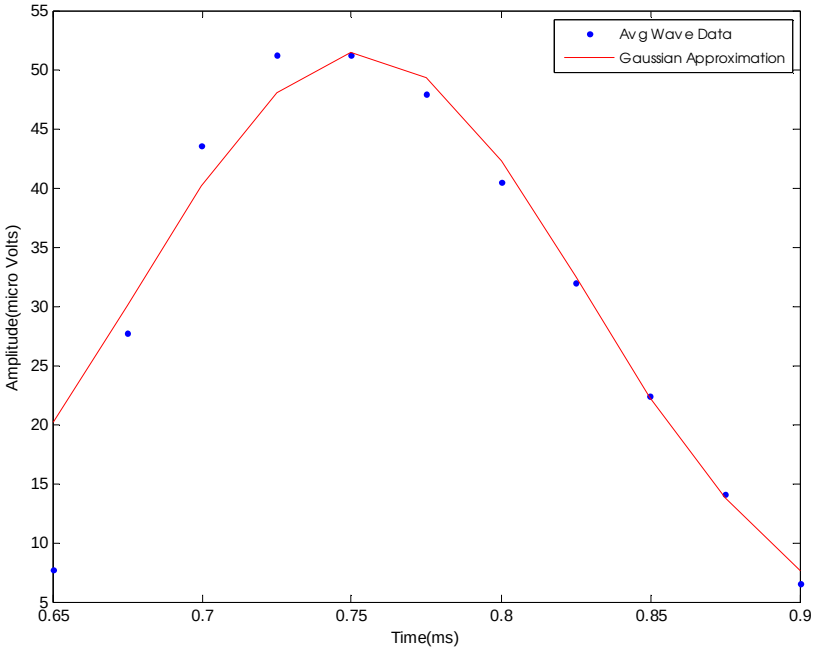

Figure 4.3: Representation of Phase 3 of Action Potential with a Gaussian Approximation curve fitting method

Table 4.1: Comparison of the Area under the curve using existing Triangular Method and an alternate approach using Gaussian Approximation Method

Rat Number	Signal Number	Day	Modality	Area using Triangular Method			Area using Gaussian Approximation Method		
				Area Phase 1	Area Phase 2	Area Phase 3	Area Phase 1	Area Phase 2	Area Phase 3
T1-R61	sig005a	28	Wake	2.6278	8.63533	10.2406	4.522	10.6786	10.6643
T1-R68	sig001a	28	Mechanical Left	2.6365	6.52619	6.47123	2.6018	8.0076	6.6283
T1-R68	sig001a	28	Heat Left	3.43716	5.67429	7.75455	2.8823	7.2301	7.6899
T1-R68	sig005b	28	Heat Left	1.87326	6.18531	7.892911	1.1072	7.3938	8.2879
T1-R68	sig001a	28	Wake	1.54916	6.50746	6.91111	2.2042	7.5483	8.6256
T1-R61	sig005a	28	Heat Left	2.2216	5.84440	7.76804	1.8479	7.4879	8.336
T1-R68	sig005b	28	Mechanical Left	2.23184	5.90112	9.17117	1.87	7.43	6.76

A possible approach to modify the current experimental design for interfacing sensory modalities and cater to the insufficiency of the data set is, pure sensory interfacing of the Sural nerve with prior identification of the different nerve fibers using conduction velocity measurements. This will enable recognition of the recording

electrodes corresponding to the activated identified nerve fiber. Application of mechanical and thermal stimulus to the skin will then readily correlate to the activity recorded during stimulation. In contrast, an Optogenetic based method in combination with electrophysiology and neuro-imaging methods such as fMRI, can be incorporated such that photo-stimulating the skin can enable uncovering of various sensory modalities and facilitate study of complex tactile perception. This method can be tested on rat models like ChR2V+ (DRG neurons expressing ChR2V) to reveal the working of the somatosensory system, using different frequencies of LED light to distinctly photostimulate specific nerve endings without effecting other receptors types.

Further, characterization of the sensory modalities can be done using wave shape signatures. Eventually, this reference waveform can be used as “training set” for a smart artificial neural network such that it is programmed to then decode the activity input from a mixed nerve.

4.1 Artificial Neural Network

Artificial Neural Network can be defined in a broad sense as an intelligent mathematical model which involves simple interconnected processing units called artificial neurons which produces a certain set of outputs based on a set of inputs. The model is trained with a given training set. Training set is an example set of input elements and expected output elements. Using this training set, the weights are calculated. These weights are then used to find the output set after processing the input set. There are different techniques that can be used to train the model to find the weights. One of the well known algorithms called back propagation algorithm (Rumelhart et al. 1986) can be used to find the relationship between the sensory modalities with respect to various wave properties i.e. Amplitude, Instantaneous Firing Frequency and Mean Inter-spike Interval.

This algorithm is based on gradient descent technique. This technique, ideally, can be used to classify any data and approximate any linear or non linear functions.

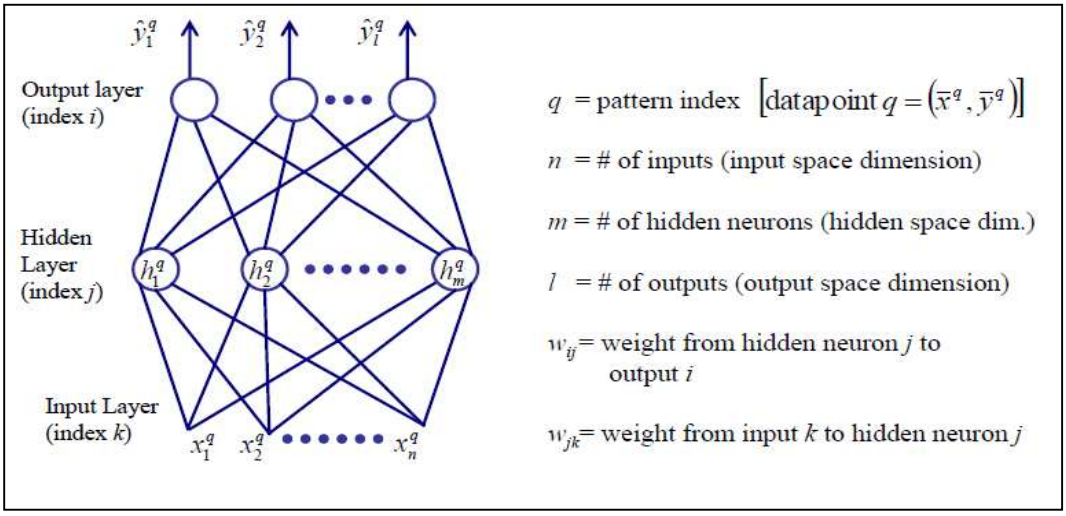

Figure 4.4: Typical Back Propagation Model

Figure 4.4 represents a general model of Back Propagation. It typically consists of three layers. They are 1) Input layer 2) Hidden layer and 3) Output layer. The simplest form of learning procedure is to present an input vector to the input layer with the size of the input layer of neuron equivalent to size of input vector. Based on the definitions in the Figure 4.4, current value or the state of the hidden layer is defined by the formula $h_j^q = f_j(\sum_{k=1}^{n} w_{jk} x_k^q)$. Similarly, state of the output layer is defined by the formula $\hat{y}_i^q = f_i(\sum_{j=1}^{m} w_{ij} h_j^q)$. The function f represents a sigmoidal function or a hyperbolic tangent function (*tanh*) function.

The above formula just represents a simple weighted sum equation which forms the basis of back propagation algorithm. The output layer produces a 'y' vector with the size equivalent to number of required outputs for the system that is in consideration. This actual output vector is compared with the desired output vector in order to obtain the error function. A simple formula representing the total error function is given by $E =$

$\frac{1}{2}\sum_c \sum_j (y_{j,c} - d_{j,c})^2$, where c = index over cases(input-output pairs), j is an index over output units and y is an actual state of an output unit and d is the desired state of the output unit. The gradient descent technique as mentioned earlier is a method to minimize this error E with respect to each weight in the network. Therefore, the aim is to find the set of weights such that, for each input vector, the output vector obtained is exactly same or sufficiently close to the desired output vector. By doing a standard derivative method, an optimal solution for the weight correction can be obtained. The correction of the weights for the output – hidden layer is given by $w_{ij} = w_{ij} + \gamma_o \delta_i^q h_j^q$, where γ_o represents learning rate. The weight update for the hidden – input layer is given by $w_{jk} = w_{jk} + \gamma_h \delta_j^q x_k^q$ (Rumelhart et al. 1986).

Based on the above formulae, this research proposes to use the ANN – Back Propagation technique to realize the relationship between sensory modalities and wave properties. To propose this model to current application, an example scenario can be considered where in a relation has to be found between the sensory modalities such as Wake, Heat and Mechanical with the wave properties such as Amplitude, Average Firing Rate, Median Inter-Spike Interval, Day. The following steps are involved in finding out the relation.

Step 1: Define Training Data

a) Inputs (x_k): Amplitude, Average Firing Rate, Median Inter spike Interval, Day
b) Outputs (y_i): Heat, Mechanical, Wake
c) No. of output neurons = 3, no. of hidden neurons = 25, no. of input neurons = 4

Step 2: Initializing the weights and other tuning parameters.

a) w_{ij}, w_{jk} to random numbers

b) Learning rate(γ) = 0.2(a value much less than 1) – tuning parameter

c) Outputs defined in the binary format(y_j): Heat(01), Mechanical(10) and Wake(11)

Step 3: Back Propagation and Weight Update by iteration

a) Calculate state of the layer(explained earlier) – using activation function such as ***tanh***

b) Define threshold for this function – Tuning parameter

c) Find $\delta_i = (y_{desired} - y_i)* f'_i$, $\delta_j = (h_{desired} - h_j)* f'_j$

d) Update the weights based on the weight update formulae discussed earlier

Step 4: Test the network based on updated weights.

The above algorithm is a representation of simple back propagation model. Step 4 can either result in a very good output that is much comparable to the desired output or it can be faulty. To optimize the algorithm, the tuning parameters such as learning rate, activation function – threshold value needs to be adjusted. Although not completely successful, an attempt was made to apply this algorithm using MATLAB program to find the relationship between the sensory modalities and wave parameters.

Appendix A

MATLAB Program for Spike Sorting and Wave Shape analysis

```
%% PLX_Spike_Analysis_3_spikeshape
%
% % Last Edit: October 31, 2012
%
% % Previous Edition
clear;clc; clear all; close all;
%-----------------------------------------------------------------
% Description of program.
%
%% This 1st module of the program is intended to extract sorted
waveforms from .PLX files and return the average peak-to-peak
voltage, average firing rate, mean and median inter-spike
interval and depolarization time of the average waveforms.
%% It exports statistics on the waveforms to a Microsoft excel
file.
%-----------------------------------------------------------------
%% Caution
%% This programs calls subroutines that are provided by plexon. %
%% This is not a standalone code.

%% Import .PLX file (name).

% Prompt user to select .PLX file.
% The uigetfile command opens a browse window.
[filename, pathname, filterindex] = uigetfile('*.plx','Select
.PLX file');
% Build a string containing full path and filename.
plxfilenameandlocation = strcat(pathname, filename);
pfl = plxfilenameandlocation;

fprintf(1,'\n  You have chosen the following file:  \n  %s
\n\n', filename);

%%

% Collect information of sorted waveforms
[tscounts, wfcounts, evcounts] = plx_info(plxfilenameandlocation,
0);
[nsc,samplecounts] = plx_adchan_samplecounts(pfl);
time_length = samplecounts(1)/40000;

fprintf(1,'\n  The following channels contain sorted waveforms:
')
for k = 18:33
    for kk = 2:5
        if wfcounts(kk,k) ~= 0
            k3 = k - 17;
            if kk==2;k4='a';end;  if kk==3;k4='b';end;
            if kk==4;k4='c';end;  if kk==5;k4='d';end;
```

```
            fprintf(1,'\n     Channel number: %g, Unit: %s.
Number of waveforms: %g.  ',k3,k4,wfcounts(kk,k))
        end
    end
end

%% Selection of signal for analysis:

% Prompt user for channel/unit:
channel = input('\n\n  Which channel [number] would you like to
analyze?  \n   ');
unitletter = input('\n  Which unit [letter] would you like to
analyze?  \n   ','s');

% Convert channel and unit into a string for output:
if channel <= 9
 chstr = strcat('sig00',num2str(channel),unitletter);
end
if channel >= 10
 chstr = strcat('sig0',num2str(channel),unitletter);
end

% Convert unit into a number:
if unitletter == 'a'; unit = 1; end
if unitletter == 'b'; unit = 2; end
if unitletter == 'c'; unit = 3; end
if unitletter == 'd'; unit = 4; end

%% Ask user for information:

rat_number = input('\n  Enter the number of the rat (ex: ''T4-
R74'').\n  ','s');
rat_day = input('\n  Enter the recording day (ex: 14).\n  ');
rat_style = input('\n  Enter the style of recording (ex: ''wake''
or ''pre'').\n  ', 's');

%% Import waveform data from .PLX file:
% (a trick here:  should be 'channel+17' and 'unit+1', but gets
adjusted inside the 'plx_waves' function.)

[n, npw, ts, wave] = plx_waves_v(plxfilenameandlocation,
channel+16, unit);
wave = wave*1000; % Adjust to microvolts.
%% Computations:

% Compute average waveform and peak-to-peak voltage.
avg_wave = mean(wave);
Vpp = max(avg_wave) - min(avg_wave);
```

```
% Compute median interspike interval.
interspike_intervals = ts*0;
for k = 2 : length(ts)
    interspike_intervals(k) = ts(k) - ts(k-1);
    mii = median(interspike_intervals);
    meanisi = mean(interspike_intervals);
end

%% Plot the waveforms

% Build time array:
% Time is in milliseconds.
t = 0 : npw-1;
t = t/40000*1000;
%%%%%%%%%%%%% End of old code%%%%%%%%%%%%%%%%%%%

%% Added Features into the old code

%% Program to find the depolarization time of the average
waveform
i = 1;
[y_min,t_min] = min(avg_wave(i,:));
min_peak_time = t(t_min);

j = t_min;
while avg_wave(i,j-1) > avg_wave(i,j)
    max_peak_time = t(j-1);
    j = j-1;
end
peak_val_1 = avg_wave(i,j);

%Finding the zero crossing in between 2nd peak and the next
minimum point
%after this peak
start_temp_data0 = j;
temp_data_0 = j;
flag = 0;
while avg_wave(i,temp_data_0-1) > avg_wave(1)

    if avg_wave(i,temp_data_0-1) == avg_wave(i,temp_data_0)
        rep_catch0 = temp_data_0;
        flag = 1;
        temp_data_0 = temp_data_0-1;
        continue;
    end
    min_time_before_first_peak = t(temp_data_0-1);
    temp_data_0 = temp_data_0-1;
end
```

```
temp_j_data_0 = start_temp_data0;
if flag == 0
    x_data_0 = t(temp_data_0-1:start_temp_data0);
    y_data_0 = avg_wave(i,temp_data_0-1:start_temp_data0);
else
    x_data_0 = [t(temp_data_0-1:rep_catch1)
t(rep_catch1+2:start_temp_data0)];
    y_data_0 = [avg_wave(i,stemp_data_0-1:rep_catch1)
avg_wave(i,rep_catch1+2:start_temp_data0)];
end

%Curve fitting from 1st peak - min point
x_data_1 = t(j:t_min);
y_data_1 = avg_wave(i,j:t_min);
h_fit1 = fittype('a1*x + a2');
fit1 =
fit(x_data_1',y_data_1',h_fit1,'StartPoint',[x_data_1(length(x_da
ta_1)) y_data_1(length(y_data_1))]);
slope1 = fit1.a1;

j = t_min
while avg_wave(i,j+1) > avg_wave(i,j)
    max_peak_time_second = t(j+1);
    j = j+1;
end
t_min
peak_val_2 = avg_wave(i,j);

% Curve Fitting from min point - 2nd peak
x_data_2 = t(t_min:j);
y_data_2 = avg_wave(i,t_min:j);
h_fit2 = fittype('a3*x + a4');
fit2 = fit(x_data_2',y_data_2',h_fit2,'StartPoint',[x_data_2(1)
y_data_2(1)]);
slope2 = fit2.a3;

%Finding the zero crossing in between 2nd peak and the next
minimum point
%after this peak
start_temp_data3 = j;
flag = 0;
while avg_wave(i,j+1) > avg_wave(1)

    if avg_wave(i,j+1) == avg_wave(i,j)
        rep_catch = j;
        flag = 1;
        j = j+1;
        continue;
    end
```

```
    min_time_after_second_peak = t(j+1);
    j = j+1;
end
temp_j_data_3 = j;

if flag == 0
    x_data_3 = t(start_temp_data3:j+1);
    y_data_3 = avg_wave(i,start_temp_data3:j+1);
else
    x_data_3 = [t(start_temp_data3:rep_catch)
t(rep_catch+2:j+1)];
    y_data_3 = [avg_wave(i,start_temp_data3:rep_catch)
avg_wave(i,rep_catch+2:j+1)];
end

%%Uncomment the below 2 lines if you want to find the slope
without curve
%%fitting
% slope1 = (peak_val_1 - y_min)/(max_peak_time - t(t_min));
% slope2 = (peak_val_2 - y_min)/(max_peak_time_second -
t(t_min));
depol_time = min_peak_time - max_peak_time;

%%
% Plot all waveforms:
subplot(2,1,1)
plot(t,wave)
titlestring1 = strcat('Channel  ', num2str(chstr),'. Total of
',num2str(n),' sorted waveforms.');
titlestring1 = ([ 'Channel ' num2str(chstr) '. Total of '
num2str(n) ' sorted waveforms.' ]);
title(titlestring1);
xlabel('Time (milliseconds)');
ylabel('Amplitude (microVolts)');
ylim([ (min(min(wave))*1.2) (max(max(wave))*1.3) ]);

% Plot average waveform:
subplot(2,1,2)
plot(t,avg_wave)
titlestring2 = ([ 'Averaged Waveform.  Amplitude =  '
num2str(Vpp) ' microVolts, peak-to-peak.' ]);
%title('Averaged Waveform.  Amplitude = %g milliVolts, peak-to-
peak.', Vpp);
title(titlestring2);
xlabel('Time (milliseconds)');
ylabel('Amplitude (microVolts)');
ylim([ (min(min(wave))*1.2) (max(max(wave))*1.3) ]);

%Plot for the curve fitting
```

```
hold on;
plot(fit1,'r-',x_data_1,y_data_1,'k.')
plot(fit2,'r-',x_data_2,y_data_2,'k.')

%Plot for just the line between 1st peak - min - 2nd peak
%Uncomment below 2 lines if you do not want to see this plot
hold on;
plot([max_peak_time t(t_min) max_peak_time_second], [peak_val_1
y_min peak_val_2]);


figure
plot(t,avg_wave)
titlestring2 = ([ 'Averaged Waveform.  Amplitude =  '
num2str(Vpp) ' microVolts, peak-to-peak.' ]);
%title('Averaged Waveform.  Amplitude = %g milliVolts, peak-to-
peak.', Vpp);
title(titlestring2);
xlabel('Time (milliseconds)');
ylabel('Amplitude (microVolts)');
ylim([ (min(min(wave))*1.2) (max(max(wave))*1.3) ]);

hold on;
plot([0 1.4],[avg_wave(1) avg_wave(1)])
xi = interp1(y_data_2,x_data_2,avg_wave(1),'linear');
temp = xi;
hold on; plot([xi max_peak_time_second],[avg_wave(1)
peak_val_2],'k--')
T3 = xi;

%%Elevation of the peaks -> Perpendicular distance between peak
and zeroth
%%line
perp_dist_1 = peak_val_1 - avg_wave(1)
perp_dist_2 = avg_wave(1) - y_min
perp_dist_3 = peak_val_2 - avg_wave(1)

xi = interp1(y_data_1,x_data_1,avg_wave(1),'linear');
T2 = xi;
hold on; plot([xi max_peak_time],[avg_wave(1) peak_val_1],'k--')
hold on; plot([xi t(t_min)],[avg_wave(1) y_min],'k--')
hold on; plot([t(t_min) temp],[y_min avg_wave(1)],'k--')

xi = interp1(y_data_3,x_data_3,avg_wave(1),'linear');
hold on; plot([t(start_temp_data3) xi],[peak_val_2
avg_wave(1)],'k--');
T4 = xi;
```

```
xi = interp1(y_data_0,x_data_0,avg_wave(1),'linear');
hold on; plot([xi t(start_temp_data0)],[avg_wave(1)
peak_val_1],'k--');
T1 = xi;

%%Zero Crossing Time difference calculation 1-2-3-4 -> Distances
from 1st
%%crossing to 2nd represented by T_12 similarly between 2-3 and
3-4 represented
%%by T_23 and T_34 respectively

T_12 = T2 - T1
T_23 = T3 - T2
T_34 = T4 - T3

Phase_1_Ydata = avg_wave(find(T1 <= t & t <= T2));
Phase_1_Xdata = t(find(T1 <= t & t <= T2));

Phase_2_Ydata = avg_wave(find(T2 <= t & t <= T3));
Phase_2_Xdata = t(find(T2 <= t & t <= T3));

Phase_3_Ydata = avg_wave(find(T3 <= t & t <= T4));
Phase_3_Xdata = t(find(T3 <= t & t <= T4));

%% data
x_1 = Phase_1_Xdata;
y_1 = Phase_1_Ydata;
x_2 = Phase_2_Xdata;
y_2 = Phase_2_Ydata*(-1);
x_3 = Phase_3_Xdata;
y_3 = Phase_3_Ydata;
%% Curve fitting
figure;
plot(x_1,y_1,'.');
%% Gaussian Function Fit
[sigmaNew,muNew,Anew]=mygaussfit(x_1,y_1);
y_new_1=Anew*exp(-(x_1-muNew).^2/(2*sigmaNew^2));
hold on; plot(x_1,y_new_1,'r');
F = @(x) Anew*exp(-(x-muNew).^2/(2*sigmaNew^2));
r1 = quad(F, x_1(1), x_1(length(x_1)));

figure;
plot(x_2,-y_2,'.');
[sigmaNew,muNew,Anew]=mygaussfit(x_2,y_2);
y_new_2=Anew*exp(-(x_2-muNew).^2/(2*sigmaNew^2));
hold on; plot(x_2,-y_new_2,'r');
F = @(x) Anew*exp(-(x-muNew).^2/(2*sigmaNew^2));
r2 = quad(F, x_2(1), x_2(length(x_2)));
```

```
figure;
plot(x_3,y_3,'.');
[sigmaNew,muNew,Anew]=mygaussfit(x_3,y_3);
y_new_3=Anew*exp(-(x_3-muNew).^2/(2*sigmaNew^2));
hold on; plot(x_3,y_new_3,'r');
F = @(x) Anew*exp(-(x-muNew).^2/(2*sigmaNew^2));
r3 = quad(F, x_3(1), x_3(length(x_3)));

%% Report

% Report number of waveforms within this waveform channel.
fprintf(1,'\n\n  The signal %s contains %g waveforms. \n', chstr,
wfcounts((unit+1),(channel+17)));

% Report average peak-to-peak voltage.
fprintf(1,'\n  The average peak-to-peak voltage is %g
millivolts.\n\n\n', Vpp);

fprintf(1,'  Results:  \n');
fprintf(1,'   Channel:                          %s \n', chstr);
fprintf(1,'   Total # of spikes:                %g sorted spikes
\n', n);
fprintf(1,'   Average spike amplitude:          %g microVolts
\n', Vpp);
fprintf(1,'   Total time length of recording:   %g seconds \n',
time_length);
fprintf(1,'   Average firing rate:              %g spikes/second
\n', (n/time_length));
fprintf(1,'   Median interspike interval:       %g milliseconds
\n', mii*1000);
fprintf(1,'   Mean interspike interval:       %g milliseconds
\n', meanisi*1000);
fprintf(1,'   Average Depolarization time:       %g milliseconds
\n',depol_time );

fprintf(1,'\n\n');

%% Output.

output = 1;
if output == 1
%  fn = ('');
 fn = ('I:\ND\Matlab_extracted_New.xlsx');
 [A, sheets, format] = xlsfinfo(fn);
 [num,txt,raw] = xlsread(fn);
 S = size(raw);
 starting_line = S(1) + 1;
 %date_today = num2str(date);
```

```
 new_line = { rat_number chstr rat_day rat_style filename n Vpp
time_length n/time_length mii*1000 meanisi*1000 depol_time};
 raw(starting_line,:) = new_line;
 %raw(starting_line,:) = [ new_line' avg_wave' ];
 %xls_start = ([ 'A' num2str(starting_line) ]);
 %xls_stop = ([ 'BN' num2str(starting_line) ]);
 %xls_range = ([ 'A' num2str(starting_line) ':BN'
num2str(starting_line) ]);
 %xlswrite(fn,[ new_line{:} avg_wave ], xls_range);
 xlswrite(fn, raw);
 fprintf(1,'\n  The above results have been added to the file
%s.\n\n\n', fn);
end

if output == 1
 fn1 = ('I:\ND\Wave_shape_21-28.xlsx');
 [A1, sheets1, format1] = xlsfinfo(fn1);
 [num1,txt1,raw1] = xlsread(fn1);
 S1 = size(raw1);
 starting_line1 = S1(1) + 1;
 %date_today = num2str(date);
 new_line1 = {rat_number chstr rat_day rat_style filename T_12
T_23 T_34 perp_dist_1 perp_dist_2 perp_dist_3};
 raw1(starting_line1,:) = new_line1;
 %raw(starting_line,:) = [ new_line' avg_wave' ];
 %xls_start = ([ 'A' num2str(starting_line) ]);
 %xls_stop = ([ 'BN' num2str(starting_line) ]);
 %xls_range = ([ 'A' num2str(starting_line) ':BN'
num2str(starting_line) ]);
 %xlswrite(fn,[ new_line{:} avg_wave ], xls_range);
 xlswrite(fn1, raw1);
 fprintf(1,'\n  The above results have been added to the file
%s.\n\n\n', fn1);
end

%% Done
```

References

Abe I, Tsujino A, Hara Y, Ichimura H, Ochiai N. Paranodal demyelination by gradual nerve stretch can be repaired by elongation of internodes. Acta Neuropatho.104 (5):505-512, 2002.

Adee S. A Manhattan Project for the Next Generation Bionic Arms. IEEE Spectrum, 2008.

Adee S. Dean Kamen's 'Luke Arm' Prosthesis Readies for Clinical Trials**.** IEEE Spectrum, 2008.

Adrian E D. The Basis of Sensation: The Action of the Sense Organs. London: Christophers, 1928.

Aleccia J. Limb loss a grim, growing global crisis. Retrieved May 7, 2010, from http://haitiamputees.msnbc.msn.com/_news/2010/03/19/4040341-limb-loss-a-grim-growing-global-crisis, 2010.

Barbieri R, Wilson M A, Frank L M, Brown E N. An analysis of hippocampal spatio-temporal representations using a Bayesian algorithm for neural spike train decoding. IEEE Trans Neural Syst Rehabil Eng 13: 131-136, 2005.

Behrend C, Reizner W, Marchessault J A, Hammert W C. Update on Advances in Upper Extremity Prosthetics: The Journal of Hand Surgery 36(10): 1711-1717, 2011.

Benke T A. Studies in Nerve Electrophysiology. MS Thesis. Rice University, 1989

Berger H. Über das Elektrenkephalogramm des Menschen, European Archives of Psychiatry and Clinical Neuroscience Volume 87: Issue 1: 527-570, 1929.

Billock J. Upper Limb Prosthetic Terminal Devices: Hands Versus Hooks. Clinical Prosthetics and Orthotics 10(2): 57-65, 1986.

Blenk K H, Michaelis M, Vogel C, Ja¨nig W. Thermosensitivity of acutely axotomized sensory nerve fibers. J. Neurophysiol. 76, 743–752, 1996.

Boretius T, Badia J, Pascual-Font A, Schuettler M, Navarro X, Yoshida K, Stieglitz T. A transverse intrafascicular multichannel electrode (TIME) to interface with the peripheral nerve. Biosensors and Bioelectronics, vol 26: Issue 1, pp 62-69, 2010.

Bradley R M, Cao X, Akin T, Najafi K. Long term chronic recordings from peripheral sensory fibers using a sieve electrode array. J. Neuro. Methods 73(2):177–86, 1997.

Branner A, Normann R. A multielectrode array for intrafascicular recording and stimulation in sciatic nerve of cats. Brain Research Bulletin, vol 51: Issue 4, pp 293-306, 2000.

Branner A, Stein R B, Fernandez E, Aoyagi Y, Normann R A. Long-term stimulation and recording with a penetrating microelectrode array in cat sciatic nerve. IEEE Trans Biomed Eng 51: 146-157, 2004.

Branner A, Stein R B, Fernandez E, Aoyagi Y, Normann R A. Long-term stimulation and recording with a penetrating microelectrode array in cat sciatic nerve. IEEE Trans. Biomed. Eng. 51:146–57, 2004.

Brushart T M, Mathur V, Sood R, Koschorke G M. Dispersion of regenerating axons across enclosed neural gaps, J Hand Surg Am. 20(4):557-64, 1995.

Burnett M, Zager E. Pathophysiology of peripheral nerve injury: a brief review. Neurosurg Focus, 16(5): Article 1, 2004.

Carlos E, Fidone S J. Physiology of the Nervous System. 2nd ed. Chicago Yearbook Medical Publishers, 1975.

Chestek C A, Gilja V, Nuyujukian P, Foster J D, Fan J M, Kaufman M T, Churchland M M, Rivera-Alvidrez Z, Cunningham J P, Ryu S I, Shenoy K V. Long-term stability of neural prosthetic control signals from silicon cortical arrays in rhesus macaque motor cortex, J. Neural Eng. 8 045005, 2011.

Cohen I, Miles R. Contributions of intrinsic and synaptic activities to the generation of neuronal discharges in *in vitro* hippocampus. The Journal of Physiology, Vol. 524, Issue 2, pages 485–502, 2000.

Cox C L, Lee S H. Excitatory actions of peptide histadine isoleucine on thalamic relay neurons. Neuropharmacology 55(8):1329–39, 2008.

Dario P, Garzella P, Toro M, Micera S, Alavi M, Meyer U, Valderrama E, Sebastiani L, Ghelarducci B, Mazzoni C, Pastacaldi P. Neural interfaces for regenerated nerve stimulation and recording. IEEE Trans Rehabil Eng. 6:353–363, 1998.

Dayan P, Abbott L. Neural Encoding I: Firing Rates and Spike Statistics, Theoretical Neuroscience, 2000.

Del V M, Cobo T, Cobo J, Vega J. Mechanosensory neurons, cutaneous mechanoreceptors and putative mechanoproteins. Microscopy Research and Technique, 2012.

Devor M. Response of nerves to injury in relation to neuropathic pain. In: McMahon SB, Koltzenburg M (eds) Wall and Melzacks textbook of pain, 5th edn. Churchill Livingstone, Edinburgh, pp 905–928, 2006.

Devor M, Seltzer Z. Pathophysiology of damaged nerves in realtion to chronic pain, P.D. Wall, R. Melzack (Eds.), Textbook of Pain, Churchill Livingstone, Edinburgh, pp. 129–164, 1999.

Dhillon G S, Horch K W. Direct neural sensory feedback and control of a prosthetic arm. IEEE Trans. Neural Syst. Rehabil. Eng. 13: 468, 2005.

Dhillon G, Horch K. Direct neural sensory feedback and control of a prosthetic arm, Neural Systems and Rehabilitation Engineering. IEEE.13(3): 468-472, 2005.

Dillingham T R, Pezzin L E, MacKenzie E J. Limb Amputatuion and Limb Defeciency: Epidemiology and Recent Trends in the United States. Souther Medical Journal 95: 875-83, 2002.

Djouhri L, Fang X, Koutsikou S, Lawson S. Partial nerve injury induces electrophysiological changes in conducting (uninjured) nociceptive and nonnociceptive DRG neurons: Possible relationships to aspects of peripheral neuropathic pain and paresthesias, Pain 2012.

Ducker T B. Metabolic factors in surgery of peripheral nerves. The Surgical Clinics of North America 52(5):1109-22, 1972.

Duncan I D. Peripheral nerve disease in the dog and cat. Vet Clin North Am Small Anim Pract 10(1):177-211, 1980.

Durand D M, Lertmanorat Z. A novel electrode array for diameter-dependent control of axonal excitability: a simulation study. IEEE Trans Biomed Eng. 51(7):1242-50, 2004.

Edell D J. A peripheral nerve information transducer for amputees: long-term multichannel recordings from rabbit peripheral nerves. IEEE Trans. Biomed. Eng. 33:203–14, 1986.

Elkoura G, Singh K. Handrix: Animating the Human Hand. Eurographics/SIGGRAPH , Symposium on Computer Animation, 2003.

Evarts E V. Pyramidal tract activity associated with a conditioned hand movement in the monkey. J _europhysiol 29: 1011-1027, 1966.

Fawcett J W, Keynes R J. Peripheral nerve regeneration. Annu Rev Neurosci. 13: 43-60, 1990.

Flanagan J R, Johansson R S. Hand Movements. Encyclopedia of the Human Brain, Elsevier Science (USA). Vol. 2: 399-414, 2002.

Fletcher I. Upper limb amputations. Br J Hosp Med 4: 590-5, 1970.

Fowler SS, Leonetti JP, Banich JC, Lee JM, Wurster R, Young MR. Duration of neuronal stretch correlates with functional loss. Otolaryngol Head Neck Surg, 124(6):641-644, 2001

Garde K, Keefer E, Botterman B, Galvan P, Romero M I. Early interfaced neural activity from chronic amputated nerves. Frontiers in Neuroengineering 2, 2009.

Gee M D, Lynn B, Basile S, Pierau F K, Cotsell B. The relationship between axonal spike shape and functional modality in cutaneous c-fibres in the pig and rat. Neuroscience Vol. 90, No. 2, pp. 509–518, 1999.

Gee M, Lynn B, Basile S, Pierau K, Cotsell B. The relationship between axonal spike shape and functional modality in cutaneous C-fibers in the pig and rat. Neuroscience Vol. 90, No. 2, pp. 509–518, 1999.

Georgopoulos A P, Schwartz A B, Kettner R E. Neuronal population coding of movement direction. Science 233: 1416-1419, 1986.

Gire D H, Schoppa N E. Long-Term Enhancement of Synchronized Oscillations by Adrenergic Receptor Activation in the Olfactory Bulb. J Neurophysiol 99:(4) 2021-2025, 2008.

Gitter A, Bosker G. Upper and Lower Extremity Prosthetics. 4th ed. Volume II. Philadelphia: Lippincott-Raven. 2005.

Gold C, Henze D A, Koch C, Buzsaki G. On the origin of the extracellular action potential waveform: a modeling study. J Neurophysiol. 95:3113–28, 2006.

Goldman L. The effects of stretch on impulse propagation in the median giant fiber of Lumbricus. J. cell. comp. Physiol. 62: 105-112, 1963.

Gonzalez C, Rodriguez M. A flexible perforated microelectrode array probe for action potential recording in nerve and muscle tissues. J Neuroscience Methods 72: 189-195, 1997.

Görke K, Pierau F K. Spike potentials and membrane properties of dorsal root ganglion cells in pigeons. Pflügers Arch. 386: 21–28, 1980.

Gorodetskaya N, Constantin C, Ja¨nig W. Ectopic activity in cutaneous regenerating afferent nerve fibers following nerve lesion in the rat. Eur J Neurosci 18:2487–2497, 2003.

Govrin-Lippmann R, Devor M. Ongoing Activity in Severed Nerves: Source and Variation with Time. Brain Research 159: 406-410, 1978.

Graham K, MacKenzie E J, Ephraim P L, Travison T G, Brookmeyer R. Estimating the Prevalence of Limb Loss in the United States: 2005 to 2050. Archives of Physical Medicine and Rehabilitation. 89(3):422-9, 2008.

Grossmann L, Gorodetskaya N, Teliban A, Baron R, Ja¨nig W. Cutaneous afferent C-fibers regenerating along the distal nerve stump after crush lesion show two types of cold sensitivity. Eur J Pain, 2008.

Guyton A C. Structure and Function of the Nervous System. 2nd ed. Philadelphia, WB Saunders, 1976.

Handwerker H O, Brune K. Deutschsprachige Klassiker der Schmerzforshung-Classical German Contributions to Pain Research, Tagblatt-Druckerei KG, Hassfurt, 1987.

Harper A A, Lawson S N. Electrical properties of rat dorsal root ganglion neurones with different peripheral nerve conduction velocities. J. Physiol. 359: 47–63, 1985.

Heger H, Millstein S, Grodon H A. Electrically powered prostheses for the adult with an upper limb amputation, British Editorial Society of Bone and Joint Surgery. 0301-620X 85 2016, 1985.

Heiduschka P, Thanos S. Implantable bioelectronic interfaces for lost nerve functions. Prog Neurobiol 55:433–461, 1998.

Heiduschka P, Thanos S. Implantable bioelectronic interfaces for lost nerve functions. Progress in Neurobiology. vol. 55, Issue 5: 433-461, 1998.

Hensel H, Boman K. Afferent impulses in cutaneous sensory nerves in human subjects. J. Neurophysiol. 23:564–578, 1960.

Henze D, Borhegyi Z, Csicsvari J, Mamiya A, Harris K, Buzsáki G. Intracellular Features Predicted by Extracellular Recordings in the Hippocampus in Vivo. J Neurophysiol. 84:390-400, 2000.

Herberts P, Körner L, Caine K, Wensby L. Rehabilitation of unilateral below-elbow amputees with myoelectric prostheses. 12(3): 123-8, 1980.

Hijjawi J B, Kuiken T A, Lipschutz R D, Miller L A, Stubblefield K A, Dumanian G A. Improved myoelectric prosthesis control accomplished using multiple nerve transfers. Plast Reconstr Surg. 118(7):1573-1578, 2006.

Hill D, Mehta S, Kleinfeld D. Quality metrics to accompany spike sorting of extracellular signals. J Neurosci. June 15; 31(24): 8699–8705, 2011.

Hochberg L R, Serruya M D, Friehs G M, Mukand J A, Saleh M, Caplan A H, Branner A, Chen D, Penn R D, Donoghue J P. Neuronal ensemble control of prosthetic devices by a human with tetraplegia. Nature 442:164-171, 2006.

Hodgkin A L, Huxley A F. A quantitative description of membrane current and its application to conduction and excitation in nerve. Journal of Physiology 117: 500–544, 1952.

Hodgkin A. A note on conduction velocity. J. Physiol. 125: 221-224, 1954.

Hsiao S S, Fettiplace M, Darbandi B. Sensory feedback for upper limb prostheses. Prog Brain Res. 192: 69-81, 2011.

Hunter G A. Amputation of the arm in adults: surgery and prosthetic fitting. Current Orthopaedics 10:121-127, 1996.

Jafari S S, Nielson M, Graham D I, Maxwell W L. Axonal cytoskeletal changes after nondisruptive axonal injury. II. Intermediate sized axons. J Neurotrauma.15 (11):955-966, 1998.

Johansson R S, Vallbo A B. Tactile sensibility in the human hand: Relative and absolute densities of four types of mechanoreceptive units in glabrous skin. J. Physiol. 286: pp 283 – 300, 1979.

Jones S W. Neuronal Firing Pattern Modulation. In: eLS. John Wiley & Sons Ltd, Chichester. http://www.els.net [doi: 10.1038/npg.els.0000174], 2001.

Jou I M, Lai K A, Shen C L, Yamano Y. Changes in conduction, blood flow, histology, and neurological status following acute nerve-stretch injury induced by femoral lengthening. J Orthop Res.18 (1):149-155, 2000.

Kandel E R, Schwartz J H, Jessell T M. Principles of Neural Science 4th ed. New York: McGraw-Hill, 2000.

Kim Y T, Romero-Ortega M I. Material Considerations for Peripheral Nerve Interfacing, MRS Bulletin. Volume 37(06), pp 573 -580, 2012.

Kubanek J, Miller K J, Ojemann J G, Wolpaw J R, Schalk G. Decoding flexion of individual fingers using electro cortico graphic signals in humans. J Neural Eng. 6:66001, 2009.

Kuiken T A, Childress D S, Rymer W Z. The hyper-reinnervation of rat skeletal muscle, Brain Surgery 676, 113-123, 1995.

Kuiken T A, Dumanian G A, Lipschutz R D, Miller L A, Stubblefield K A. The use of targeted muscle reinnervation for improved myoelectric prosthesis control in a bilateral shoulder disarticulation amputee. Prosthet Orthot Int. 28(3):245-253, 2004.

Kuiken T A, Dumanian G A, Lipschutz R D, Miller L A, Stubblefield K A. The use of targeted muscle reinnervation for improved myoelectric prosthesis control in a bilateral shoulder disarticulation amputee. 28(3): 245-53, 2004.

Kuiken T A, Miller L A, Lipschutz R D, Lock B A, Stubblefield K, Marasco PD, Zhou P, Dumanian G A. Targeted reinnervation for enhanced prosthetic arm function in a woman with a proximal amputation: a case study. Lancet. 3: 369(9559):371-80, 2007

Kuiken T A. Consideration of nerve-muscle grafts to improve the control of artificial arms. Technol Disabil: 15105-111, 2003.

Kuiken T A. Targeted reinnervation for improved prosthetic function. Phys Med Rehabil Clin N Am.17(1):1-13, 2006.

Kwan M K, Wall E J, Massie J, Garfin S R. Strain, stress and stretch of peripheral nerve Rabbit experiments in vitro and in vivo. Acta Orthopaedica. 63: 267-272, 1992.

Le Bars D, Gozariu M, Cadden S. Animal Models of Nociception, Pharmacological Review 53:597–652, 2001.

Lebedev M A, Nicolelis M A L. Brain–machine interfaces: past, present and future. Trends in Neurosciences 29(9): 536-546, 2006.

Liu X, Eschenfelder S, Blenk K, JaÈnig W, HaÈbler H. Spontaneous activity of axotomized afferent neurons after L5 spinal nerve injury in rats. Pain 84:309 - 318. 2000.

Light C, Chappell P, Kyberd P. Establishing a Standardized Clinical Assessment Tool of Pathologic and Prosthetic Hand Function: Normative Data, Reliability, and Validity. Arch Phys Med Rehabil Vol 83, 2002.

Lotfi P, Garde K, Chouhan A K, Bengali E, Romero-Ortega M I. Modality-specific axonal regeneration: toward selective regenerative neural interfaces. Frontiers in Neuroengineering: 4(11), 2011.

Magee D J. Orthopedic physical assessment. Philadelphia: W B Saunders, 1997.

Manzano G M, Lydia M P, Giuliano J A M, Nóbrega. A brief historical note on the classification of nerve fibers. Arq Neuropsiquiatr; 66(1):117-119, 2008.

Marks W B, Loeb G E. Action currents, internodal potentials, and extracellular records of myelinated mammalian nerve-fibers derived from node potentials. Biophys. J. 16:655–68, 1976.

Mattia M, Ferraina S and Giudice PD. Dissociated multi-unit activity and local field potentials: A theory inspired analysis of a motor decision task. NeuroImage 52: 812-823, 2010.

Maxwell W L, Graham D I. Loss of axonal microtubules and neurofilaments after stretch-injury to guinea pig optic nerve fibers. J Neurotrauma 14(9):603-614, 1997.

McMahon S B, Bennett D L H, Bevan S. Inflammatory mediators and modulators of pain. In: McMahon SB, Koltzenburg M (eds) Wall and Melzacks textbook of pain, 5th edn. Elsevier Churchill Livingstone, Edinburgh, pp 49–72, 2006.

McNaughton T G, Horch K W. Metallized polymer fibers as leadwires and intrafascicular microelectrodes. J Neuroscience Methods 70:103–110, 1996.

McNeal D R. Analysis of a model for excitation of myelinated nerve. IEEE Trans. Biomed. Eng. 23:329–37, 1976.

Merrill D R, Tresco P A. Impedance characterization of microarray recording electrodes in vitro. IEEE Trans Biomed Eng. 52(11):1960-5, 2005.

Micera S, Carpaneto J, Raspopovic S. Control of Hand Prostheses Using Peripheral Information. IEEE Reviews in Biomedical Engineering 3: 48-68, 2010.

Millesi H, Zoch G, Reihsner R. Mechanical properties of peripheral nerves. Clinical Orthop Relat Res. 314:76– 83, 1995.

Moiseenkova V, Bell B, Motamedi M, Wozniak E, Christensen B. Wide-band spectral tuning of heat receptors in the pit organ of the copperhead snake (Crotalinae). Am J Physiol Regul Integr Comp Physiol 284:R598-R606, 2003.

Navarro X, Calvet S, Butı´M, Go´mez N, Cabruja E, Garrido P, Villa R, Valderrama E. Peripheral nerve regeneration through microelectrode arrays based on silicon technology. Restor Neurol Neurosci. 9:151–160, 1996.

Navarro. X, Krueger T B, Lago N, Micera S, Stieglitz T, Dario P. A critical review of interfaces with the peripheral nervous system for the control of neuroprostheses and hybrid bionic systems. Journal of the Peripheral Nervous System, Volume 10, Issue 3, pages 229–258, 2005.

Noguchi K, Kawai Y, Fukuoka T, Senba E, Miki K. Substance P induced by peripheral nerve injury in primary afferent neurons and its effect on dorsal column nucleus neurons. J Neurosci 15:7633 - 7643, 1995.

Oh S S, Hayes J M, Sims-Robinson C, Sullivan K A, Feldman E L. The effects of anesthesia on measures of nerve conduction velocity in male C57Bl6/J mice. Neurosci Lett. 483(2):127-31, 2010.

Paninski L, Fellows M R, Hatsopoulos N G, Donoghue J P. Spatiotemporal tuning of motor cortical neurons for hand position and velocity. J Neurophysiol 91: 515-532, 2004.

Parent A. Carpenter's human neuroanatomy. 9th Ed. Baltimore: Williams & Wilkins, 1996.

Proske U, Iggo A, Luff A R. Mechanical sensitivity of regenerating myelinated skin and muscle afferents in the cat. Exp Brain Res. 104: pp. 89–98, 1995.

Purves D, Augustine G, Fitzpatrick D, Hall W, Samuel-Lamantia A, Mcnamara J, Williams S. Neuroscience. pp. 207–209, 2004.

Quiroga Q. What is the real shape of extracellular spikes? Journal of Neuroscience Methods 177:194–198, 2009.

Raffe M R. Peripheral Nerve injuries in the dog, Part II. Compendium on Continuing Education for the small Animal Practitioner 1:269-276, 1979.

Ramer M S, Bisby M A. Rapid sprouting of sympathetic axons in dorsal root ganglia of rats with a chronic constriction injury. Pain 70:237 - 244, 1997.

Rumelhart D E, Hinton G E, Williams R J. Learning Representations by Back Propagatin Errors. Nature. Vol. 323: 533-536, 1986.

Rutten W L C. Selective electrical interfaces with the nervous system. Ann Rev Biomed Eng 4:407–452, 2002.

Schmidt C E, Leach J B. Neural tissue engineering: strategies for repair and regeneration. Annual Review Biomed Eng 5: 293-347, 2003.

Schultz A E, Kuiken T A. Neural Interfaces for Control of Upper Limb Prostheses: The State of the Art and Future Possibilities, PM&R. vol 3:Issue 1, 2011.

Schwartz A B, Cui X T, Weber D J, Moran D W. Brain-controlled interfaces: Movement restoration with neural prosthetics. Neuron. 52:205–220, 2006.

Smit J P A, Rutten W L C, Boom H B K. Endoneural selective stimulation using wire-microelectrode arrays. IEEE Trans. Rehabil. Eng. 7:399–412, 1999.

Stecker M, Baylor K, Wolfe J, Stevenson M. Acute nerve stretch and the compound motor action potential. Journal of Brachial Plexus and Peripheral Nerve Injury. 6:4, 2011.

Stein R B, Walley M. Functional comparison of upper extremity amputees using myoelectric and conventional prostheses. Arch Phys Med Rehabil 64(6):243-8, 1983.

Stewart J D. Peripheral nerve fascicles: Anatomy and clinical relevance. Muscle & Nerve vol. 28: Issue 5, pages 525–541, 2003.

Struijk J J, Thomsen M, Larsen J O, Sinkjaer T. Cuff electrodes for long-term recording of natural sensory information—studying the relationship between nerve damage and electrophysiological parameters in long-term implants. IEEE Eng. Med. Biol. Mag. 18:91–98, 1999.

Tarkka I M, Hallett M. The cortical potential related to sensory feedback from voluntary movements shows somatotopic organization of the supplementary motor area. Brain Topogr. 3(3):359-63, 1991.

Thurston A J. Paré and prosthetics: the early history of artificial limbs. ANZ J Surg. Dec 77(12):1114-9, 2007.

Topp K, Boyd B. Structure and Biomechanics of Peripheral Nerves: Nerve Responses to Physical Stresses and Implications for Physical Therapist Practice. Physical Therapy. vol. 86(1): 92-109, 2006.

UgoBasile Dynamic Plantar Aesthesiometer Manual, Cat No. 37450, pp 14, 2012.

Vernon B. The sensory hand. Harvard University Press, Mountcastle 2005.

Vince V, Thil M A, Gérard A C, Veraart C, Delbeke J, Colin I M. Cuff electrode implantation around the sciatic nerve is associated with an upregulation of TNF-alpha and TGF-beta. J. Neuroimmunol. 159: 75, 2005.

Vitali M, Robinson K P, Andrews B G, Harris E E. Amputations and prostheses. London: Baillière Tindall.10. 1978.

Wall P, Devor M, Inbal R, Scadding J, Schonfeld D, Seltzer Z, Tomkiewicz M. Autotomy following peripheral nerve lesions: experimental anesthesia dolorosa, Pain, Volume 7, Issue 2, 103-113, 1979.

Watson R C. Investigations into Causes of Failure of Regenerative Peripheral Nerve Interfaces. PhD Diss. University of Texas Arlington. 2012.

Wedell G, Miller S. Cutaneous Sensibility, Annual Reviews 24:199-222, 1962.

Wilhelm J C, Xu M, Cucoranu D, Chmielewski S, Holmes T, Lau K S, Bassell G J, English A W. Cooperative roles of BDNF expression in neurons and Schwann cells are modulated by exercise to facilitate nerve regeneration. J. Neurosci. 32(14): 5002-9. 2012.

Wolpaw J R (Guest Editor), Birbaumer N, Heetderks W J, McFarland D J, Peckham P H, Schalk G, Donchin E, Quatrano L A, Robinson C J, Vaughan T M(Guest Editor). Brain–Computer Interface Technology: A Review of the First International Meeting, IEEE TRANSACTIONS ON REHABILITATION ENGINEERING, VOL. 8, NO. 2, 2000.

Wolpaw J R, Birbaumer N, McFarland D J, Pfurtscheller G, Vaughan T M. Brain-computer interfaces for communication and control. Clin Neurophysiol 113: 767-791, 2002.

Xu L, Furukawa S, Middlebrooks J C. Auditory cortical responses in the cat to sounds that produce spatial illusions. Nature 399: 688-691, 1999.

Yaksh T L, Hua X Y, Kalcheva I, Nozaki-Taguchi N, Marsala M. The spinal biology in humans and animals of pain states generated by persistent small afferent input. Proc Natl Acad Sci USA 96: 7680-7686, 1999.

Yeomans D, Proudfit H. Nociceptive responses to high and low rates of noxious cutaneous heating are mediated by different nociceptors in the rat: Electrophysiological evidence. Pain 68: 141-150, 1996.

Yoshida K, Jovanovic K, Stein R B. Intrafascicular electrodes for stimulations and recording from mud puppy spinal roots. J Neurosci Methods 96:47–55, 2000.

Yoshida S, Matsuda Y, Samejima A. Tetrodotoxin-resistant sodium and calcium components of action potentials in dorsal root ganglion cells of the adult mouse. J. Neurophysiol. 41: 1096–1106, 1978.

Zhong Y, Yu X, Gilbert R, Bellamkonda R. Stabilizing electrode-host interfaces: a tissue engineering approach, Journal of Rehabilitation Research and Development Vol. 38 No. 6, November/December 2001.

Biographical Information

Nilanjana T Dutta received her Bachelor's degree in Electronics Engineering from All India Shree Shivaji Memorial Society, Institute of Information Technology (A.I.S.S.M.S I.O.I.T), Pune, India, in June 2008. She then worked as a Subject Matter Expert (Team Lead) in IBM Global Services Pvt. Ltd, Pune, India for two years starting from September 2008. She began her Graduate studies in Bioengineering at University of Texas at Arlington in Fall 2010. During her studies she worked as the graduate research assistant in the Regenerative Neurobiology Laboratory and gained research experience in the field of Neurointerfacing under the mentorship of Dr. Mario I. Romero-Ortega.